

**SIMULATION AND CHARACTERIZATION OF SEPARATE
ABSORPTION AND MULTIPLICATION InGaAs/InP AVALANCHE
PHOTODIODE**

By

MAHDI ALL KHAMIS

**A Dissertation Submitted to the College of Graduate Studies, Universiti Tenaga Nasional,
in Fulfillment of the Requirements for the Degree of Master of Electrical Engineering**

DECLARATION

I hereby declare that the dissertation is my original work except for quotations and citations which have been duly acknowledged. I also declare that it has not been previously, and is not concurrently submitted for any other degree at Universiti Tenaga Nasional or at any other institutions. This dissertation may be made available within the university library and may be photocopied and loaned to other libraries for the purpose of consultation

25 September 2018

MAHDI ALL KHAMIS

SE22238

ABSTRACT

Avalanche photodiodes (APDs) are important components in the receiver module of the telecommunication system. Utilizing Indium Gallium Arsenide (InGaAs) as an absorption layer and Indium Phosphide (InP) as a multiplication layer makes the device suitable for optical fiber communication application especially in long haul communication system. The APD has gone through several evolutions in the last few decades. Each evolution has been with the purpose of increasing avalanche gain, frequency response and yield. This thesis reports a comprehensive work in designing the structure and evaluating the performance of the separate absorption, graded, charged and multiplication InGaAs/InP (SAGCM InGaAs/InP) through simulation of the APD device structure. The effect of multiplication layer width (MLW) and absorption layer width (ALW) on APD performance was studied and investigated. Silvaco TCAD software was used as simulation tools to simulate a precise model of InGaAs/InP APD and analyze its performance under illuminated conditions. As such, three different ALW with various MLW have been simulated while the structure of APD and material parameters were kept constant. It was found that in the APD with smaller MLW, the distance between the punch-through voltage and the breakdown voltage can be maximized. Therefore, the operation region of APD will be extended. In addition, the multiplication gain was calculated from the photocurrent and primary current by taking the APD collection efficiency effect under the consideration. One of the main challenges in this work was the precise physical parameters of the semiconductor materials for the simulation of dark current, photocurrent and impact ionization of the APD. Representing APD gain by considering the collection efficiency effect of APD was another major challenge. As such, extensive investigation has been performed and as a results a list of semiconductor material physical parameters which is suitable for (SAGCM) InGaAs/InP APD design using Silvaco ATLAS framework was fully established by correlating the simulation results to the experimental results. These physical parameters would be useful for future research work in optimizing the InGaAs/InP APD before going into actual semiconductor growth and APDs fabrication, which would significantly reduce the design cost of the APDs.

ACKNOWLEDGEMENT

I would like to express my sincere gratitude to my supervisor Dr. Ker Pin Jern for his kind guidance, continuous support, patience, motivation, enthusiasm and immense knowledge for the completion of this research. His valuable advice, suggestion and encouragement were key motivations throughout my Masters.

Next, I would like to thank Universiti Tenaga Nasional (UNITEN) for their technical support towards the project and I would like to thank my other courses faculty for facilitating the study.

Lastly, I am very much grateful to my beloved family, for their love, continuous encouragement and all kind of support needed to complete my study.

TABLE OF CONTENT

| | |
|---|----------|
| DECLARATION | i |
| ABSTRACT | ii |
| ACKNOWLEDGEMENT | iii |
| TABLE OF CONTENT | iv |
| LIST OF TABLES | viii |
| LIST OF FIGURES | ix |
| LIST OF PUBLICATION | xi |
| LIST OF ABBREVIATIONS | xii |
| LIST OF SYMBOLS | xiii |
| | |
| CHAPTER 1 | 1 |
| INTRODUCTION | 1 |
| 1.1 General optical communication system | 1 |
| 1.2 Optical receiver | 2 |
| 1.3 Introduction to Semiconductor Photodetectors | 2 |
| 1.3.1 Semiconductor | 3 |
| 1.3.1.1 Intrinsic semiconductor | 3 |
| 1.3.1.2 Extrinsic semiconductor | 4 |
| 1.3.2 Photodetectors | 5 |
| 1.3.2.1 Photoemissive | 9 |
| 1.3.2.2 Photoconductive | 9 |

| | | |
|-------------------|---|----|
| 1.4 | Problem Statement of the dissertation | 11 |
| 1.5 | Objectives | 12 |
| 1.6 | Scope | 12 |
| CHAPTER 2 | | 13 |
| LITERATURE REVIEW | | 13 |
| 2.1 | Fundamental of Photodetector | 13 |
| 2.1.1 | Photodetection | 13 |
| 2.1.2 | General characteristic of Photodetectors | 15 |
| 2.2 | Photodetectors without internal gain | 17 |
| 2.2.1 | P-N Photodiode | 17 |
| 2.2.2 | P-I-N photodiode | 18 |
| 2.3 | Semiconductors photodetectors with internal gain | 19 |
| 2.3.1 | Photoconductive detectors | 19 |
| 2.3.2 | Photoresistors | 20 |
| 2.4 | Fundamental to Avalanche Photodiode (APD) | 20 |
| 2.4.1 | Multiplication | 21 |
| 2.4.2 | Photocurrent | 25 |
| 2.4.3 | Noise in APD | 26 |
| 2.4.4 | Response time And Bandwidth | 29 |
| 2.5 | APD Design | 30 |
| 2.5.1 | Separate Absorption and Multiplication APD | 31 |
| 2.5.2 | Absorption Layer Width and Multiplication layer Width | 34 |
| 2.5.3 | Structure and material Parameters | 35 |
| 2.6 | Simulation | 38 |
| 2.6.1 | Simulation of APD | 40 |

| | |
|--|----|
| CHAPTER 3 | 42 |
| METHODOLOGY | 42 |
| 3.1 Device Simulation | 42 |
| 3.2 Choice of Simulation Models | 44 |
| 3.3 Device Simulation in Silvaco | 46 |
| 3.4 Gummel method | 48 |
| 3.5 Newton method | 49 |
| 3.6 Block method | 49 |
| 3.7 Silvaco ATLAS | 50 |
| 3.8 Deckbuild | 51 |
| 3.9 Basic Device Simulation | 53 |
| 3.9.1 Mesh Construction | 53 |
| 3.9.2 Region Define | 55 |
| 3.9.3 Electrodes | 57 |
| 3.9.4 Doping | 58 |
| 3.9.5 Model and method | 60 |
| 3.9.6 Light source | 62 |
| 3.10 Design of avalanche photodiode | 64 |
| CHAPTER 4 | 66 |
| RESULTS AND DISCUSSION | 66 |
| 4.1 APD operation region | 66 |
| 4.2 APD Electric field | 67 |
| 4.3 Photocurrent and Multiplication gain | 70 |
| CHAPTER 5 | 78 |
| CONCLUSION AND RECOMMENDATIONS FOR FUTURE WORK | 78 |

| | | |
|-----|-------------|----|
| 5.1 | Conclusions | 78 |
| 5.2 | Future Work | 79 |
| | REFERENCES | 80 |
| | APPENDIX A | 85 |
| | APPENDIX B | 90 |
| | APPENDIX C | 96 |

List of Tables

| | | |
|------------|---|----|
| Table 2.1: | The thicknesses and their Doping Concentrations of a few InGaAs/InP APDs. | 36 |
| Table 2.2: | SRH lifetime value. | 38 |
| Table 3.1: | Basic Atlas commands and brief description. | 52 |
| Table 3.2: | Outlines a few of the models used in Silvaco simulations. | 61 |
| Table 3.3: | Structure parameters for the main design of SAGCM InGaAs/InP ADP. | 65 |
| Table 4.1: | Material parameters of SAGCM InGaAs/InP APDs in the simulation. | 73 |
| Table 4.2: | Punch-through voltage and break down voltage values for all simulated structures with their deference for each MLW. | 75 |

List of Figures

| | | |
|--------------|---|----|
| Figure 1.1. | The optical fiber communication system [4]. | 1 |
| Figure 1.2. | Optical receiver block diagram. | 2 |
| Figure 1.3. | Silicon structure and covalent bond. | 4 |
| Figure 1.4. | The Electromagnetic Spectrum. | 6 |
| Figure 1.5. | Classification of Photodetectors. | 8 |
| Figure 1.6. | Schematic of photoconductor that made of only one type semiconductor. | 10 |
| Figure 1.7. | a) shows conventional Bipolar Junction Transistor and b) is a typical phototransistor. | 11 |
| Figure 2.1. | P-N junction depletion and diffusion regions. | 17 |
| Figure 2.2. | A front-illuminated homojunction InGaAs PIN photodiode [12]. | 18 |
| Figure 2.3. | PIN InGaAs/InP Phototransistor. | 20 |
| Figure 2.4. | Energy band diagram with Multiplication process in an APD. | 23 |
| Figure 2.5. | Block schematic of various noise sources in the optical receiver [4]. | 26 |
| Figure 2.6. | SAM p ⁺ -n-n APD structure [4]. | 31 |
| Figure 2.7. | Responsivity \mathcal{R} versus wavelength λ for number of photodiodes [3]. | 32 |
| Figure 2.8. | Separate absorption and multiplication (SAM) APD. (a) Layer composition and electric field profile (b) cross section of SAM APD [4]. | 33 |
| Figure 2.9. | Energy band diagrams for SAM and SAGM APDs [4][12]. | 34 |
| Figure 2.10. | Absorption coefficient versus Wavelength for several material [1]. | 37 |
| Figure 3.1. | The right hand side of the arrows shows the types of commands for process simulation. The left hand side shows the corresponding commands used in the Silvaco platform. | 50 |
| Figure 3.2. | Flowchart illustrating the main modules for data analysis and display. | 51 |
| Figure 3.3. | Specify the Mash in Silvaco Atlas for SAM InGaAs/InP APD. | 54 |
| Figure 3.4. | Mesh for the SAM InGaAs/InP APD. The mesh was produced in SILVACO. Proper mesh setup is necessary for accurate solutions. | 55 |
| Figure 3.5. | The regions and materials that have been assigned in this Silvaco Atlas for SAM APD simulation. | 56 |
| Figure 3.6. | The cross section of SAM structure after assigning regions and materials in the simulation. | 56 |

| | | |
|--------------|--|----|
| Figure 3.7. | Assigning the electrodes to the APD structure in two different locations. | 57 |
| Figure 3.8. | Specifying the doping profile for all regions of SAM APD in Silvaco Atlas. | 58 |
| Figure 3.9. | Cross section of the SAM APD doping profile as produce by Silvaco. | 59 |
| Figure 3.10. | Assigning the electrodes material to the structure. | 60 |
| Figure 3.11. | Display console of the models and calculation method. | 61 |
| Figure 3.12. | Display the concentration of the incident light and applied voltage. | 62 |
| Figure 3.13. | Silvaco output file showing the photogeneration rate within the device. | 63 |
| Figure 3.14. | Cross section view of main design of simulation APD. | 64 |
| Figure 4.1. | Simulated photocurrent and dark current for main APD design compare with experiment. | 67 |
| Figure 4.2. | Build-in electric field for 1.8 μm ALW with vary MLW. | 68 |
| Figure 4.3. | Built-in electric field for 2.0 μm ALW with vary MLW. | 68 |
| Figure 4.4. | Build-in electric field for 2.2 μm ALW with vary MLW. | 69 |
| Figure 4.5. | Display the I-V curves of simulated photocurrent. | 71 |
| Figure 4.6. | Display multiplication (M) versus Voltage (V) for all simulated structures. | 72 |
| Figure 4.7. | Punch-through voltage and break down voltage verses MLW for three ALW as labeled. | 76 |

LIST OF PUBLICATIONS

1. Mahdi All Khamis, W. Emilin Rashid, Pin Jern Ker, K. Y. Lau, “Effect of Multiplication and Absorption Layers Width on Avalanche Multiplication Gain in InGaAs/InP Avalanche Photodiode” International Journal of Engineering & Technology (2018). (www.sciencepubco.com/index.php/IJET. It has been accepted, presented and it will be published) – Scopus indexed journal
2. W. Emilin Rashid, Pin Jern Ker, M. Z. Jamaludin, N. A. Rahman and Mahdi All Khamis, “Optimization of p-type Emitter Thickness for GaSbBased Thermophotovoltaic Cells”, IEEE International Conference on Semiconductor Electronics 2018 (ICSE 2018), August 2018. – Scopus indexed conference proceeding

LIST OF ABBREVIATIONS

| Abbreviation | Meaning |
|---------------------|--|
| BER | Bit-Error-Rate |
| EM | Electromagnetic |
| PMT | Photo-Multiplier-Tube |
| LDR | Light Dependent Resistor |
| APD | Avalanche Photodiode |
| BJT | Bipolar Junction Transistor |
| e-h | Electron-Hole |
| SNR | Signal to Noise Ratio |
| GBW | Gain-Bandwidth Product |
| SAM | Separate Absorption and Multiplication |
| SAGM | Separate Absorption Graded and Multiplication |
| SAGCM | Separate Absorption Graded Charged and Multiplication |
| ALW | Absorption Layer Width |
| MLW | Multiplication Layer Width |
| SRH | Shockley-Hall-Reed |
| TCAD | Technology Computer Aided Design |
| ISE | Integrated Systems Engineering |
| TMA | Technology Modeling Associates |
| OS | Operation System |
| IDE | Integrated Development Environment |

LIST OF SYMBOL

| Symbol | Meaning |
|---------------|------------------------------------|
| A | amplitude |
| f | frequency |
| λ | wavelength |
| s | second |
| c | speed of light |
| h | Planck's constant |
| e | Electron |
| V | voltage |
| E_g | Energy bandgap |
| E_{Photon} | photon energy |
| ΔE | transition within the material |
| α | absorption coefficient |
| η | quantum efficiency |
| R | reflection coefficient |
| d | depth |
| ζ | fraction of carriers |
| I_d | dark current |
| I_{ph} | photocurrent |
| I_{pr} | Primarily photocurrent |
| P_{inc} | incident optical power |
| \mathcal{R} | Responsivity |
| t_r | rise time |
| C | capacitor |
| α_e | electron ionization coefficient |
| α_p | hole ionization coefficient |

| Symbol | Meaning |
|---------------|---|
| b_e | electron critical electrical field |
| b_h | hole critical electrical field |
| k | ionization coefficient ratio |
| M | multiplication gain |
| $J_{e(x)}$ | electrons current density at x position |
| $J_{h(x)}$ | hole current density at x position |
| K_B | Boltzmann constant |
| T | temperature |
| BW | Bandwidth |
| R_c | resistance of photo-conductive |
| R_{sh} | shunt resistance |
| I_{sh} | Shot noise |
| I_B | background noise |
| F_e | Electron excess noise factor |
| F_h | Hole excess noise factor |
| F | excess noise factor |
| v_e | Electron saturation velocity |
| v_h | Hole saturation velocity |
| W_d | width of absorption region |
| τ_m | multiplication time |
| q | Charge |
| E | Electric field |
| V_b | Breakdown voltage |
| V_p | Punch-through voltage |
| B | Magnetic field |

| Symbol | Meaning |
|---------------|--|
| U_n | generation rates for electrons |
| U_p | generation rates for hole |
| E_{Fn} | electron Fermi level |
| E_{Fp} | hole Fermi level |
| G | generation rate due to impact ionization |
| G_n | Electron generation rates |
| G_p | Hole generation rates |

CHAPTER 1

INTRODUCTION

1.1 General optical communication system

The basic concept of an optical fiber communication system as shown in Figure 1.1 is the same as any other communication system. They are designed for the same purpose to transmit the information from a source to a destination. In an optical fiber communication system, the electrical signal is first converted from its electrical (analog or digital) form to the optical form of signal then by the help of light emitting diode or laser as optical source, it can be transmitted over the optical fiber. Finally, an optical detector converts the receiving optical signal to its electrical form through a Photodetector.

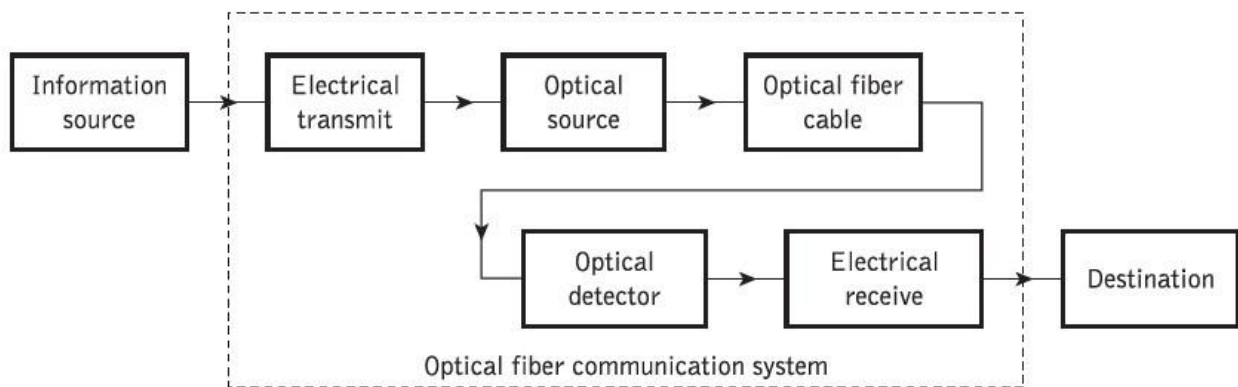


Figure 1.1. The optical fiber communication system [4].

The optical fiber communication system takes great advantage of low attenuation and very wide bandwidth characteristics of optical fiber. Generally, the communication system that use optical fiber as optical carrier wave guide, has a number of superb features such as, huge bandwidth, small

size, low loss, secure and no electromagnetic interference effect [4]. All those advantages will be achieved only when the light wave has been used as carrier through an optical fiber.

1.2 Optical receiver

The block diagram of optical receiver is shown in Figure 1.2. The receiving optical signal will be detected by the optical detector and be converted to electrical signal through the optical detector. Next the preamplifier boosts the output signal of Photodetector, and converts it into the voltage signal. The main amplifier followed by equalizer is responsible to amplify the signal to a suitable and fixed level regardless of the detector optical input power. Filter (Low Pass), as the last component, has functionality to maximize the optical receiver Signal to Noise Ratio (SNR) while it maintains the necessary characteristics of signal.

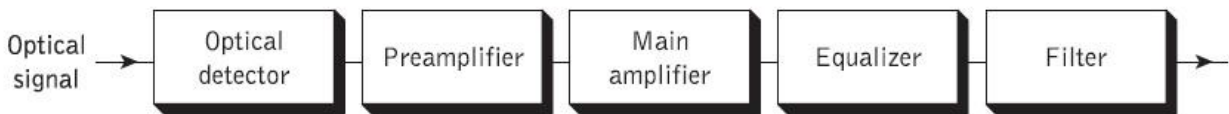


Figure 1.2. Optical receiver block diagram.

Sensitivity and bandwidth are the most important characteristics of the optical receiver. For the optical receiver, the sensitivity is defined as the minimum power that the receiver requires to operate at bit-error-rate (BER) of 10^{-9} . It has been estimated that approximately 21 incident photons are needed to have a binary 1 with BER of 10^{-9} . However, this is the fundamental minimum which may not be achieved in a practical device [4].

1.3 Introduction to Semiconductor Photodetectors

Optical electronic is about the interaction of electronic processes with photons and optical processes. Devices in which can satisfy this interaction are usually associated with an energy

conversion process (from optical to electrical and vice versa), are known as optoelectronic devices. Such devices are conventionally made of semiconductor materials. This section is discuss basic understanding of the principles of semiconductor optoelectronic materials and devices [1].

1.3.1 Semiconductor

The solid materials in electronic compare with their current carrying capacity and they can classified into the three types namely conductors, semiconductors and insulators. Conductors are the materials that have excellent current carrying capacity such as copper. Semiconductor, as the name suggest only allows partial or semi-conduction of current to pass through them. In the other words, the current carrying capacity of semiconductors is between conductors and insulators such as Silicon and Germanium. Whereas, the insulators that do not have current carrying capacity such as wood, ceramic, glass and plastic. Semiconductors are further divided into intrinsic and extrinsic semiconductors, depending their structure properties [1].

1.3.1.1 Intrinsic semiconductor

Intrinsic means in its pure form. Therefore, these types of semiconductors are in the pure form by the nature of existence, such as Silicon and Germanium. They have four valence electrons orbiting in their outer shell (Valence electrons are the electrons that associated with as atom. The one that most likely react with other atoms, form bonds, share or taking away with/by other atoms). Understanding the motion of these electrons require study of atom structure. In this case, Silicon atom is the best example as intrinsically, has four valence electrons and require the additional four electrons (total eight) to be stable and form the semiconductor structure by bonding millions of these Silicon atoms together, Figure 1.3 shown the Silicon structure. All these atoms are setup a bond with each other which is called as covalent bond. However, these bands are strong enough that the electrons are failed to break at 0 Kelvin but as the temperature increases the electrons will absorb the heat energy and they able to break the bond. Once the bond is broken the electrons are free to carry current which is lead to deficiency of an electron. Thus, there is an empty space formed that can refer to as hole.

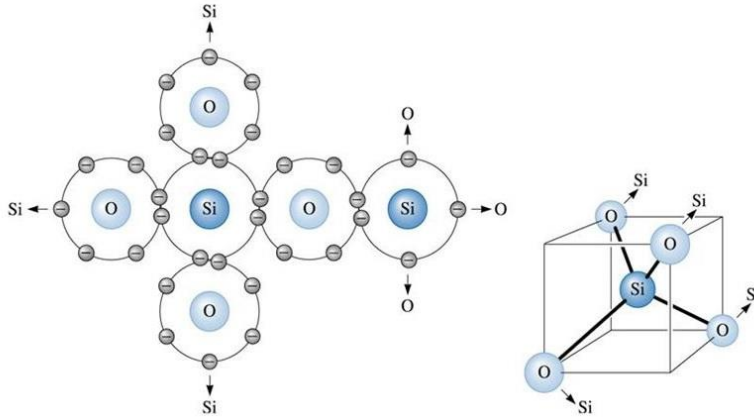


Figure 1.3. Silicon structure and covalent bond.

These holes consider having positive charge whereas, electron has negative charge. Therefore, the immediate neighboring electron gets attracted towards these holes and fills it place. This process itself creates another hole and it will be continue in entire structure in random manner.

1.3.1.2 Extrinsic semiconductor

Extrinsic semiconductors have some impurities added to them to impure their conductivity. They are further subdivided to two types P-type or trivalent which has three electrons in its outer shell such as Boron, Indium, Gallium and N-type or pentavalent which has five electrons in its outer shell such as Phosphorus and Arsenic. The process of adding impurities to the intrinsic semiconductors is called Doping. And the impurities that improve the conductivity of these semiconductors are called Dopants.

a. P-type or trivalent

In the case of P-type, the Silicon will be doped by the atoms that have three electrons in its outer shell like Boron. These three electrons of Boron will form three bonds with Silicon and fourth bond of silicon will be one hole which immediate neighboring electron will attracted towards these holes thus creating another hole in its previous location. Simultaneously, the Silicon's electrons gain thermal energy and keep breaking the covalent bonds at room temperature. Thus, creating further free electrons

and this movement will go on in the same manner. Therefore, the number of electrons generated in this structure dominates over the electrons and structure can be called as P-type semiconductor.

b. N-type or pentavalent

The atomic structure of N-type semiconductors have five electrons in outer shell and that is due to adding material that has five electrons in their last atomic layer such as Phosphorus. As silicon require only four additional electrons to achieve stability, in N-type atom there is one extra electron as a valence electron that make the N-type structure to get negative charge. This process forms four bond with Silicon atom which remain one electron that does not form any bond and remain free. Therefore, the free electron readily available for conduction. This electron rotates randomly around the N-type atom result in breaking of the bond as have been illustrated earlier.

1.3.2 Photodetectors

Photodetectors are semiconductor device that able to detect optical signals. In the other words, is a optoelectronic device that absorbs optical signals and generate electrical energy. Which usually manifests as a photocurrent. Light or optical signal can be described as a wave and as particles. In both conditions, the optical signal contains a certain amount of energy $E_{\text{photon}} (\zeta)$, (which has a direct relation with radiation frequency, shown in Equation 1.1). The detection the optical signal occurs through a very vital process of absorption or emission of photons by the semiconductor material. In general, atoms (as building of all matters) are made of three subatomic particles which are Protons, Neutrons, and Electrons. Proton and electron have positive and negative electric charge respectively. Electrons with its negative charge whiz around the nucleus (protons and neutrons) and are attracted by the positive charge of protons. Based on the modern model of atoms the electrons are only allowed to occupy very specific volumes of space around the nucleus which only depend on the electron`s energy. These specific volumes of space can be imagined as levels or steps around the nucleus. Electrons are allowed to move between these levels (up or down) by obtaining just the right and certain amount of energy. Light (optical signal) is a source of energy for electrons in semiconductor Photodetectors. Electrons can absorb this energy and be promoted to one or more steps up. It can also release that energy by emitting the light at that energy to go

down to a lower energy level too. The movement of electrons between the atoms energy levels (up or down) will generate the electrical signal (voltage or current) [3].

Light, the energy source of electrons in semiconductor photodetectors, has very special properties, which is named the wave-particle duality. It means light can behave as a wave and as a particle. Certain properties of light can best be described as wave and while other properties can best be described as a particle (which the same condition turns out to be true for electrons as well). As a wave, light is an electromagnetic (EM) wave or radiation which consists of two oscillating, mutually, perpendicular fields. One of them is the magnetic field and another one is the electric field. These two perpendicular fields propagate through space at the speed of light ($c = 3 \times 10^8$ m/s). The electromagnetic wave has three general characteristics, amplitude (A) of the wave

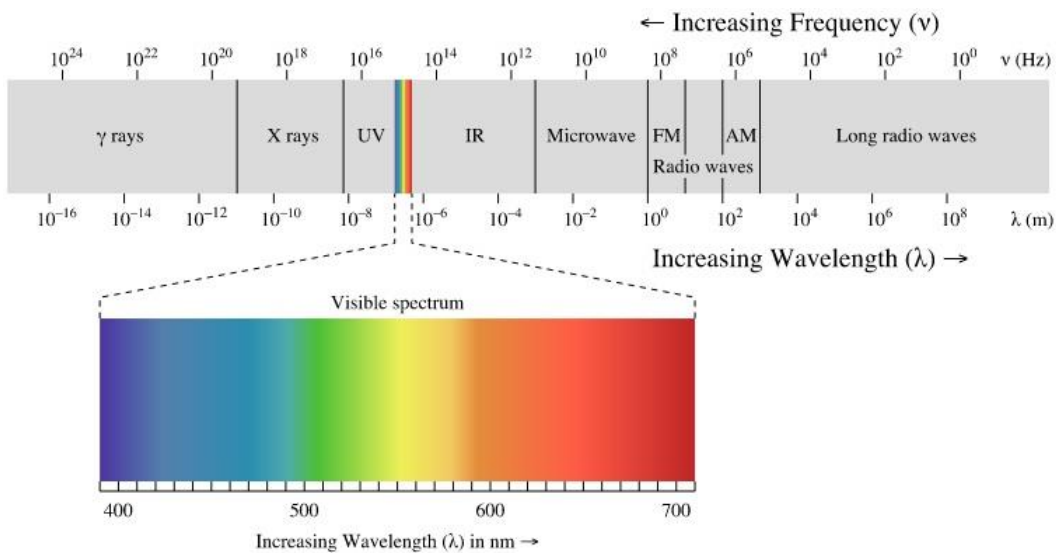


Figure 1.4. The Electromagnetic Spectrum.

which is going to determine the intensity or brightness of the light, wavelength (λ) is a distance between two adjacent crest or troughs and frequency (f) which is amount of wave cycles pass by a fixed point in a given amount of time (cycle/s). An electromagnetic wave has a large spectrum

from γ -ray to long radio waves, with a visible region from ~ 400 to 700 nm [45]. Figure 1.4 shows the EM spectrum. With increasing frequency and decreasing wavelength from the right to the left. Each λ and f corresponds to a particular energy of photon by the equation

$$E_{\text{photon}} = hf = hc/\lambda \quad (\text{Equation 1.1})$$

Where, h is the Planck's constant (6.626×10^{-34} m² kg/s) and c is the speed of light ($c = 3 \times 10^8$ m/s). The photoelectric effect is the best way to describe light as a particle. If the light with a sufficient energy shined on the piece of metal (which has intrinsic free electrons), it can break the electrons bound and generate electrons flow. In fact, the collision between light particles (photons) and electrons transfer the photons energy to the electrons and cause the electron movements which generate current. In this processes, each photon is responsible for freeing one electron from its bound. In this context, the free electron known as photoelectron. The minimum amount of energy that photon requires to free an electron is called the work function (E_0) and it can be calculated as follow:

$$E_{\text{photon}} = E_0 + KE_{\text{photoelectron}} \quad (\text{Equation 1.2})$$

Where $KE_{\text{photoelectron}}$ is kinetic energy [2].

Both of this behavior of the light have been used and taken advantage of in the process of photodetection. Photodetectors which use in thermal optics application are more depend on wave behavior of the light whereas optical communication utilizations are more depend on particle behavior of light. Generally, there are three steps involved in the photodetection process. First, absorption of light energy and generate the carriers. Second, transportation of (optical) generated carriers across the absorption (and/or transit region), with or without gain. Third, collection of carriers and generation of a photocurrent which flow through external electronic circuits. Sometimes the detection process is associated with demodulation, when converting the optical signal with high frequency into time-revolving electrical signal. Photodetectors are able to detect very wide range of the optical spectrum.

Photodetectors are very commonly used in optical communication systems. In these systems, a photodetector captures and converts the transmitted optical pulse (with minimum loss) into an electrical pulse that can be used by any electronic devices. The performance of the photodetector is evaluated on a few parameters such as low noise, wide bandwidth and high sensitivity. Also having a very cost-efficient product is always considered by the design engineers. Optical communication systems need high speed photodetectors due to the long travelling distance for the optical signal; high gain capability is needed to amplify the attenuated optical signal. Therefore, bandwidth and internal gain are two important characteristics of the photodetectors.

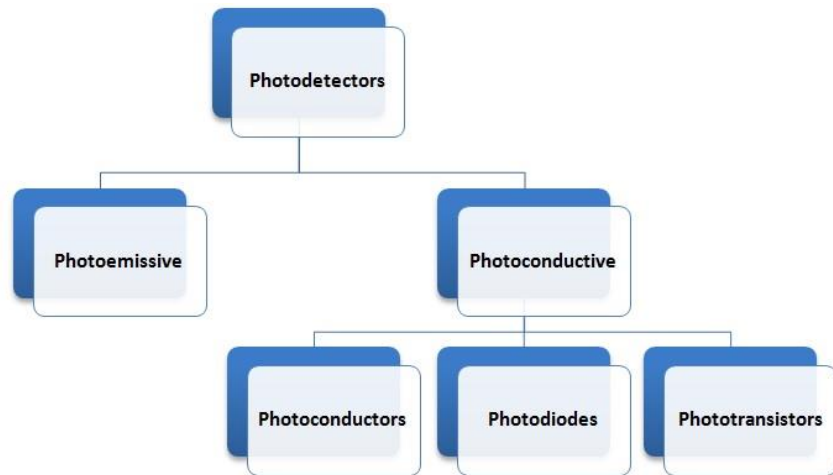


Figure 1.5. Classification of Photodetectors.

Photodetectors can be made from intrinsic or extrinsic semiconductors. For the application that uses wavelength near to the band gap of the semiconductor, an intrinsic photodetector will be used. And detection of light energy below the band gap energy usually will be done by the extrinsic photodetector [4]. Photodetectors are broadly categorized into two types, photoemissive and photoconductive. As Figure 1.5 illustrates, the photoconductive category is classified into three subcategories, photoconductor, photodiodes, and phototransistor [3]. The physical characteristics and principles of these devices will be discussed in the next chapter.

1.3.2.1 Photoemissive

In photoemissive detectors, the incident photon results in the emission of an electron. A very important example of photoemissive detectors is Photo-Multiplier-Tube (PMT). It consists of photo-cathode, anode and number of dynodes (Dynode is an electrode in vacuum tube that serves as an electron multiplier through secondary emission). When the photons strikes the photo-cathode, it free electrons which are subsequently multiplied by dynodes through avalanche process to get significant amount of current. PMTs are extremely sensitive and able to detect very low light. However PMTs inconveniently large and requires a high voltage (1000 V~ 3000 V) to operate [3].

1.3.2.2 Photoconductive

In photoconductive device the incident photon changes the conductivity of the detector. Basically, they are three types, photoconductor, photodiodes, and phototransistor. The following sections discuss each type of photoconductive detector.

a. Photoconductor

Photoconductor is a simple piece of semiconductor which is not junction device. The photoconductors operation is based on the changes in the conductivity. The photogenerated electrons and holes are attracted by opposite contacts and results in a photocurrent. The schematic of a photoconductor in its simple form, is shown in Figure 1.6. The thickness of the active layer should be large enough so that it can absorb a significant fraction of the incident photon but at same time small enough so to minimize the noise current resulting from a low resistance of the semiconductor layer.

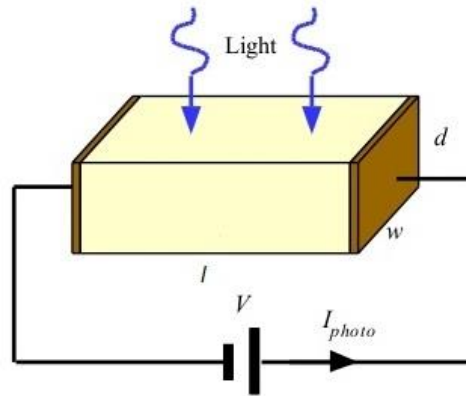


Figure 1.6. Schematic of photoconductor that made of only one type semiconductor.

One of the common application of photoconductor is to be used as a light dependent resistor (LDR) or Photoresistor. Photoresistor, is similar to a controlled variable resistor which is made of high resistance semiconductors. The conductivity or resistance in this device is proportional to the intensity of the light.

b. Photodiodes

Photodiode is a junction between positively-doped (p-type) and negatively-doped (n-type) semiconductor, often with an intrinsic or undoped region between them. Most of the photodiodes made from intrinsic semiconductor material, which require the photon with energy equal or greater than the band gap energy. The photodiode is the most commonly used Photodetection for common and specialized applications, such as optical communication since they have very fast response and high gain. There are several types of photodiodes. Some of the most important ones in this category are discussed below but the PIN photodiode (which I stands for intrinsic layer between the p-type and n-type layers) and avalanche photodiode will be discussed in details in next chapter.

c. **Phototransistor:** Phototransistor includes two parts. One part is collector PN junction and another is sensitive to the light. The phototransistor behaves similar to the conventional Bipolar Junction Transistor (BJT). The light sensitive part in phototransistor works exactly like the base in normal transistor and able to control the generated light current The only difference, as shown in Figure 1.7 (b), is that

phototransistor does not have the base connection. When the light strikes the collector-base PN junction, base current is produced which is directly proportional to the light intensity.

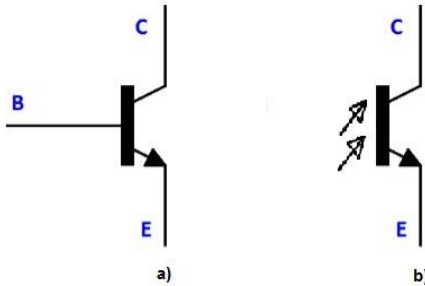


Figure 1.7. a) shows conventional Bipolar Junction Transistor and b) is a typical phototransistor.

This action itself produces collector current. They usually made from material such as gallium Arsenide. Phototransistor operates in active region. This type of detector circuit can be used for wide variety of applications that are depending on light intensity levels. The typical example is Ambient Light Detector Circuit.

1.4 Problem Statement of the dissertation

Since, the 90s [6][46] the studies of APDs focused on suitably thin multiplication layer, due to its positive effect on the performance of APD. However, there still lack of experimental data on the effect of multiplication layer width on APD performance. On the other hand, to avoid time-consuming and cost inefficient of fabrication and wafer grow of InGaAs/InP APD a precise simulation can provide equally accurate data (as experimental data) for the purpose of performance enhancement and design optimization of APDs.

1.5 Objectives

The overall or general objective of this work is to develop a simulation model that is suitable for InGaAs/InP. In order to achieve this, this work consists of the following specific objectives:

- 1- To investigate and study the optical properties and physical parameters of III-V semiconductor materials to optimize numerical simulation parameters for InGaAs/InP avalanche photodiode.
- 2- To simulate the photocurrent and dark current of InGaAs/InP avalanche photodiode under the illuminated condition using Silvaco simulator program.
- 3- To formulate the relationship and effects of absorption layer width and multiplication layer width on the gain of InGaAs/InP avalanche photodiode.

1.6 Scope

In this thesis extensive attempt and investigation will be done to simulate and model the (SAGCM) InGaAs/InP APD and its avalanche breakdown voltage. The dark current and photocurrent will be simulated based on the optical properties and physical parameters obtained through the simulation. By further analyzing the photocurrent characteristic, the avalanche gains, for different multiplication layer width and absorption layer width were investigated and analyzed. The widths of the absorption layer were confined to 1.8 μm , 2.0 μm , 2.2 μm , while those for the multiplication widths were 0.2 to 0.8 μm . The other characterizations such as frequency response and excess noise are not considered (or discussed in details) since the understanding and analysis of these parameters require more time and resources.

CHAPTER 2

LITERATURE REVIEW

2.1 Fundamental of Photodetector

Basically, Photodetectors are devices that able to absorb the energy of photon flux or optical power and convert it into proportionate electrical signal (voltage or current), so it can be measurable. There are a lot of references that have brilliant explanation about Photodetectors [2][3][4] .

2.1.1 Photodetection

As the name implies it basically detects incident photons or radiation and convert it to the electrical signals (voltage or current). This process involve three steps as follow:

- a. Incident light generate e-h carriers. If the incident light with enough energy strike the surface of material, generate carries (electron-hole pairs). This phenomena also known as photoelectric effects.
- b. Carries transport/multiplication. Once these carriers are generated they need to be transported to the respective electrodes. Sometimes, some sort of carriers multiplication, also possible to get involved which called gain.
- c. Extraction of carriers as a current. Finally, these carriers are then extracted of the device in the form of the current.

Generally there are two classes of photodetection. Photoelectric detector (Photoemissive) and thermal detector (photoconductive).

- a. The first class are the photoelectric detectors which basically photons generate electron-hole pairs. These kinds of detectors are based on photoelectric effect or Photoeffect [3]. Internal Photoeffect and external Photoeffect are the tow configuration of this operation.

The internal Photoeffect implicates photoconductivity, in which the excited electrons and holes enhance the conductivity of material by remaining in there. The external Photoeffect implicates photoemission, in which, the strike of light on the surface of material result in emission of electron. The most popular example of photoemission is photomultiplier tube (PMT) which has been discussed in section 1.3.2.1. In this thesis we are mainly dealing with this (first) class of the detectors.

- b. The second class is the thermal detectors. In this particular case by shining light to the material the temperature will raise (directly) proportional to the light that shine on the material. So, the temperature will sense when light absorbed. There are detecting mid-Infrared radiation which is mainly used for imaging application. Compared to the photoelectric emission the thermal detectors are not sufficient and very slow. However, the latest enhancement of manufacturing have increased the performance of this kind of detectors [3].

Considering incident light on the material with wavelength λ . As it has illustrated in the Equation 1-1, this light can be detected if this λ corresponding to some sort of transition with the new material. Therefore, as long as

$$\lambda \leq hc/\Delta E \quad \text{(Equation 2.1)}$$

Where ΔE is a transition within the material. Thus the λ will be detected. ΔE depends on verity of transitions which can define the wavelength range of the detector. To be more specific ΔE determines the long wavelength or the maximum wavelength that is possible. In the other words, depending upon the wavelength range that is interested in, the appropriate type of detector material can be chosen. Also any wavelength that larger than the maximum wavelength that is determined will not be able to produce the electron-hole pairs and not get absorb. On the other hand, the lower wavelength determine by the term called absorption coefficient (α). Because the wavelength is related to the energy and the energy can be compare to the bandgap energy, therefore, can relate the absorption coefficient to the wavelength by considering the α as function of λ as follow ($\alpha = f(\lambda)$)

$$\alpha = \frac{4\pi\bar{k}}{\lambda} \quad (\text{Equation 2.2})$$

Where the \bar{k} is the extinction coefficient.

2.1.2 General characteristic of Photodetectors

The general characteristics appropriate for all Photodetectors are the following.

a. Quantum efficiency Responsivity

The quantum efficiency η ($0 \leq \eta \leq 1$) is referred to as the fraction number of carriers generated (with no gain) per incident photons. This process can be 100% efficient which means every incident photon can generate one electron-hole pair, or the efficiency can be less than 100%. The η depends on the reflection coefficient (R), depth (d), absorption coefficient (α) and finally, ζ the fraction of carriers (electron-hole pair) that can contribute to the output current of the detector. Therefore, the quantum efficiency can be written as

$$\eta = (1 - R)(1 - \exp(-\alpha d))\zeta \quad (\text{Equation 2.3})$$

As discussed in Sec. 2.1.1, α is the absorption coefficient that depends on the wavelength, thus the quantum efficiency is a function of the wavelength as well. This can lead to the following equation [1]

$$\eta = \frac{\frac{I_{ph}}{e}}{\frac{P_{inc}}{h\nu}} = \frac{I_{ph}}{P_{inc}} \frac{hc}{e\lambda} \quad (\text{Equation 2.4})$$

Where, e is electron charge, P_{inc} is incident optical power and I_{ph} is a photocurrent

b. Responsivity

The Responsivity (\mathcal{R}) is defined as the photocurrent generated (I_{ph}) over the incident optical power P_{inc} therefore, it has a direct relation with quantum efficiency. And it is illustrated as the following equation [1]:

$$\mathcal{R} = \frac{I_{ph}}{P_{inc}} \quad (\text{Equation 2.5})$$

From equations 2.2 and 2.3, as Responsivity as a function of quantum efficiency can simply be defined as follow

$$\mathcal{R} = \eta \frac{\lambda}{1.24} \quad (\text{Equation 2.6})$$

The Responsivity has unit of A/W and λ is in μm . The equation 2.4 illustrate that for an incident optical power, the maximum photocurrent can be generated, only if the quantum efficiency is maximized.

c. Rise time (t_r)

Impulse response refers to response of the detector or system to an input impulse, (an instantaneous impulse). The two important factors to determine impulse response are 1) the transit time of carriers (t_r). 2) RC time constant by the external circuit, which include the RC of the detector itself too. The t_r of the carriers determines the speed of response, which means how fast the detector is and also lead to the determination of the bandwidth of the detector [3].

d. Noise Power or Dark current

Basically, noise is random fluctuation in an electrical signal. In terms of photodetector it is called dark current or noise power which refers to the temperature dependent current that flows in a photodetector when no light is shining on it.

e. Internal Gain

Gain is defined as the ratio of number of collected carriers to the number of carriers that correspond to the Photodetector current.

2.2 Photodetectors without internal gain

This kind of semiconductor photodetector provides no internal gain and the most popular of this type of photodetector, usually consisted of an intrinsic region, which is located between two highly doped p-type and n-type semiconductor.

2.2.1 P-N Photodiode

Basically, a P-N photodiode functions under reverse bias (negative side of power supply connect to P side and positive connect to N side), and photon could be absorb in both depletion region (region that electron movement is based on potential different) and diffusion region (region that electron movement is based on concentration different) as illustrated in Figure 2.1. Electron and holes are getting separated and drifted away in the depletion region by mean of electric field (potential different). Within diffusion region the pairs slowly spread to depletion region and finally generate current. Some portion of the carriers recombines in diffusion region and do not contribute to the generated external current. Thus, lager depletion region lead to higher quantum efficiency. This also makes the capacitance smaller in the P-N junction which result in higher bandwidth characteristic. However, to avoid long drift time of carriers in depletion region, this area cannot be too large; otherwise, it will affect the bandwidth by increasing the respond time of the P-N junction.

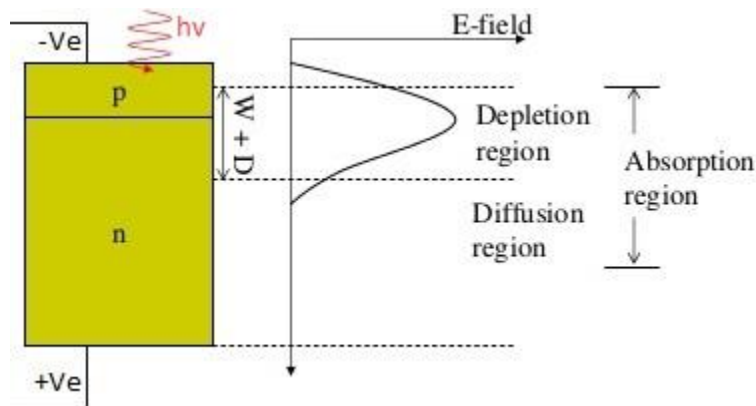


Figure 2.1. P-N junction depletion and diffusion regions.

This is actually, exemplifies the relationship between gain and speed of response in all kind of photodetectors.

2.2.2 P-I-N photodiode

Almost all detectors which are used in high speed application are PIN photodiodes and also it is one of the well-known photodetectors without internal gain in optical communication. PIN photodiodes (P-I-N) as Figure 2.2 shows have displaced PN photodiode since they can achieve quantum efficiency and bandwidth in optimum level and also easy to fabricate. The other reasons that PIN photodiodes are widely used is because they relatively low noise and high reliable.

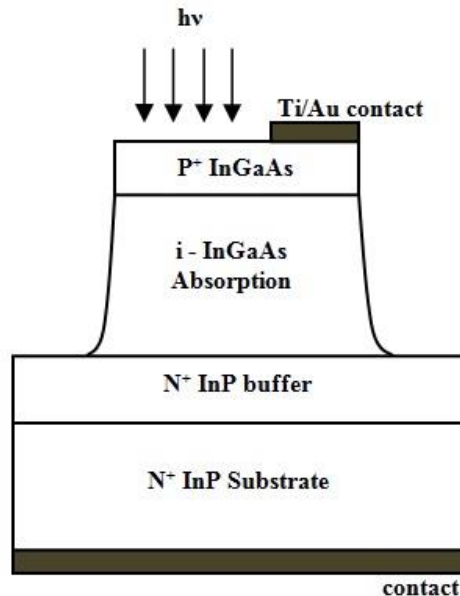


Figure 2.2. A front-illuminated homojunction InGaAs PIN photodiode [12].

The carrier collection process in PIN photodiode is fast and effective since all the creation of the carriers are occur in depletion region, thus, the natural bandwidth is going to be very high (because of extrinsic effects the bandwidth typically limited up to a few tens of GHz) [12]. The top layer (P⁺ InGaAs) in the surface of PIN photodiodes hast to be fairly thin to reduce the penetration loss. Otherwise, the surface recombination is going to be strong and this will destroy the quantum efficiency. There are a few solutions to avoid such a disaster. In case of single heterojunction,

solution is to create an optical window under the bottom layer (N^+ InP Substrate) and change the PIN photodiode front-illuminated to back-illuminated photodiode, since the InP is transparent to wavelength longer than $0.92 \mu\text{m}$ [12]. Another way is to make the structure double heterojunction by replacing the thin layer of P^+ InGaAs to thick layer of N^+ InP.

2.3 Semiconductors photodetectors with internal gain

This type of photodetector has abilities to internally amplify the signal by increasing conductivity or utilizing impact ionization mechanize process due to the high electric field. One of the well-known photodetector with internal gain is the avalanche photodiode, which will be discussed in details in the next section.

2.3.1 Photoconductive detectors

The semiconductor material (such as InGaAs) has been used as absorption layer in a photoconductive detector. The functionality of this kind of detectors is based on increasing the conductivity of detector in the presence of the incident photon due to the generation of carriers which increases the current. However, they expected to have very limited dark current in the dark and at fixed voltage bias. The carriers generated will move with different speed towards the respective electrodes. The carriers with the higher speed collected first, which lead to the excessive charge in the photodetector. Also, this excessive charge will draw faster electrons and holes pairs into the conductive layer, and this process will continue until the slower carriers are recombined or eventually collected. Thus, the internal gain of the photodetector can be calculated as $\frac{t}{t_r}$ which t is the transmit time of slower carriers (lifetime) and t_r is the transmit time of faster carriers [3]. In terms of optical communication, the high dark current and its relative noise are the main problems. Since the quantum efficiency would be significantly affected by these to problems, the bandwidth will be limited as well. Therefore, the photoconductive detectors are hardly used in optical communication.

2.3.2 Photoresistors

A bipolar transistor and a photo-resistor are resemblant, except there is on an electrode to the base of photo-resistor as illustrated in Figure 2.3. In the photo-resistor, the base-collector junction area is design to be sensitive to photons (photosensitive). In the base region, the holes which generated in the photosensitive region are accumulated. Like the typical bipolar transistor, the extreme charges motivate the electrons to move from emitter and cause the current gain. Photo-resistors have been investigated since 1977 and yet not be trusted to be used in main optical communication system [12][3]. It is because they do not have sufficient fast rise time and their amplification are not linear enough to meet the requirement of steady-state illumination [12].

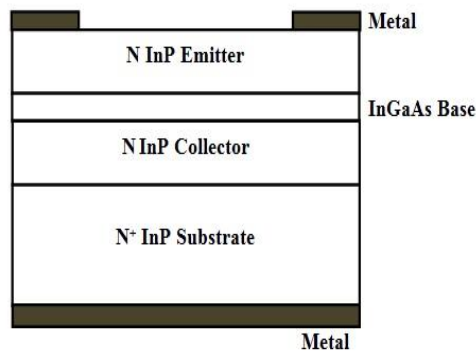


Figure 2.3. PIN InGaAs/InP Phototransistor.

2.4 Fundamental to Avalanche Photodiode (APD)

Avalanche photodiode has the capability to multiply the number of electron-hole (e-h) pairs generated by the incident photons. This device operates under the reverse bias in which electric field of the depletion region is high. The generated carrier can, therefore, obtain sufficiently high energy to excite new carriers (e-h) pairs through impact ionization process. From the structure point of view, APDs are basically a PIN diode but with large reverse bias, which provide avalanche gain. Comparing to the PIN diode, APDs have four main differences as follow [2][3][4]:

- a. Relatively large reverse bias required (30 V ~ 70 V)
- b. A built-in gain in the device due to carrier multiplication process in depletion or active region.

- c. Higher photocurrent, typical gain of $M \sim 10 - 100$
- d. Higher sensitivity, but noisier.

2.4.1 Multiplication

When dealing with devices that utilize avalanche breakdown as a gain mechanism it becomes necessary to take a closer look at the theory of multiplication gain and the accurate way to mathematically describe this process, which is based on impact ionization process. M. H. Wood and W. C. Johnson [48] described two equal methods for APD gain calculation: steady-state point of view and transit case (where initiation is done by the fixed number of carriers). In this thesis, the steady-state point of view has been adapted for analyzing APD gain. In this method, the current distribution of electrons and holes are examined respectively, with taking high electric field region and collection efficiency of APD under the consideration.

In most modern-day semiconductor devices, impact ionization is an undesired process. When impact ionization begins to occur in a semiconductor device it is usually referred to as having reached a state of breakdown which is undesirable in a solid state. However, APDs are devices that take advantage of the point where impact ionization occurs and experiences breakdown.

The amount of energy that the particles (electrons) required to leave or be removed from atom called ionization energy and defined by ionization coefficient α (α_e is represent the electron ionization coefficient and α_h is represent hole ionization coefficient). The reverse of this coefficient $\frac{1}{\alpha}$ ($\frac{1}{\alpha_e}$ and $\frac{1}{\alpha_h}$) represent the average space between continuous ionization. Furthermore, the ionization coefficient ratio (k) as one of the main parameters to characterizing the APD performance is defined as [3]

$$k = \frac{\alpha_e}{\alpha_h} \quad \text{(Equation 2.7)}$$

In the presence of electric field, higher energy can be obtained by the carriers due to the acceleration of particles and therefore, impact with other particles. It has been proven

[1][14][22][23][35] that the impact ionization for very straightforward model (for example for large area diode) can be expressed as a function electric field base on Selberherr method by the following equations.

$$\alpha(E) = \alpha_e e^{(-\frac{b_e}{E})C_e} \quad (\text{Equation 2.8})$$

$$\beta(E) = \alpha_h e^{(-\frac{b_h}{E})C_h} \quad (\text{Equation 2.9})$$

Where, $b_{e,h}$ and $C_{e,h}$ are the critical electrical field and defined on the IMPACT statement respectively [34]. These parameters are also arbitrary and dependent on the impact ionization numerical calculation methods, some of these parameters ($b_{e,h}$, $C_{e,h}$) can be ignored or eliminated.

To be more specific, in semiconductor devices, when an electron is removed from the valence band to the conduction band by means of energy transfer from another electron, impact ionization occurs. When an electron enters an electric field in a semiconductor it will begin to drift through that semiconductor in the opposite direction of the electric field. As it travels through the electric field, its drift velocity depends on the strength of the field. Eventually, the average drift velocity of electrons present in the field reaches a point of saturation known as the saturation velocity. Increasing the strength of the electric field beyond this point will not increase the average drift velocity of the electrons in the material, due to the collisions and interactions between the free electrons and the lattice, but it will increase the average energy of these free electrons. In the presence of these large electric fields, the energy of electrons that interact with the crystal lattice can be larger than the threshold energy. When this happens the electrons transfer their energy through impact ionization events. This process is illustrated in Figure 2.4. (In the other words) as it is illustrated, because of the large reverse bias, the potential barrier or potential energy diagram has a large slope in the depletion region. Due to this large potential barrier, when the incident photon creates electron-hole pair, the electron will travel down in the slope and as they move down they accelerated and gain kinetic energy. The kinetic energy of the electron will knock down another electron and create additional carrier pair by the avalanche process. Similarly, at the same time, the holes are also accelerated up towards the P side and create secondary electron-hole pairs which lead to creating gain; that is increasing number of carriers by avalanche process. This

process continued until all electron-hole pairs move out of the high electric region. Eventually, one initial carrier (e-h) generates M additional carrier (e-h) pairs. Thus, M is defined as APDs' (photogain) carrier multiplication gain [1][2][3]. To mathematically determine the M in APD in which both electron and hole carriers are responsible of carrier multiplication (M), we consider electron carriers only then expand the equation for hole carriers (If $\alpha_h = 0$, the ratio of ionization coefficients $k = \frac{\alpha_h}{\alpha_e} = 0$).

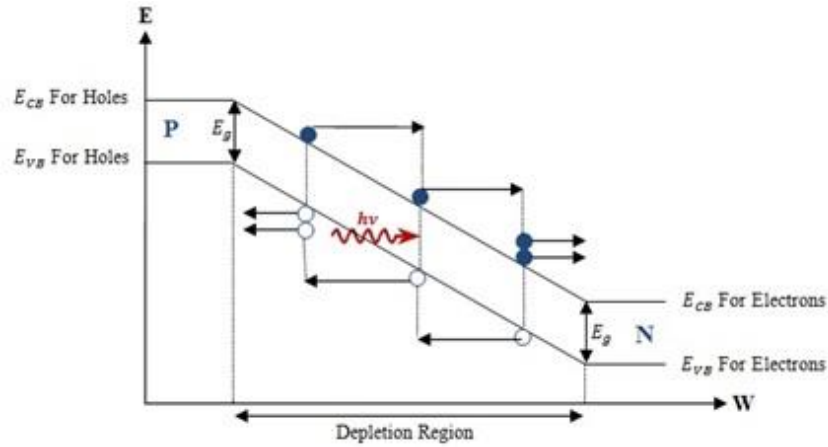


Figure 2.4. Energy band diagram with Multiplication process in an APD.

Thus the electrons electric current density at x position ($J_e(x)$), can be defined as follow:

$$dJ_e(x) = \alpha_e J_e(x) dx \quad (\text{Equation 2.10})$$

$$\frac{dJ_e}{dx} = \alpha_e J_e(x) \quad (\text{Equation 2.11})$$

Which has exponential solution as $J_e(x) = J_e(0) \exp(\alpha_e x)$. Therefore, the M is

$$M = \exp(\alpha_e W) \quad (\text{Equation 2.12})$$

Where W is the thickness of multiplication layer.

Now by adding $J_h(x)$ (the hole current density) to the Equation 2.9, it can be rewritten as

$$\frac{dJ_e}{dx} = \alpha_e J_e(x) + \alpha_h J_h(x) \quad (\text{Equation 2.13})$$

The $J_e(x) + J_h(x)$ should remain constant for all the x position under steady-state condition (because of the charge neutrality, $dJ_e/dx = -dJ_h/dx$). If assume that the multiplication layer is n-type then, there are no holes injected in this region ($J_h(W) = 0, x = W$). Therefore, by eliminating the $J_h(x)$ from Equation 2.11, it can be written as

$$\frac{dJ_e}{dx} = (\alpha_e - \alpha_h)J_e(x) + \alpha_h J_h(W) \quad (\text{Equation 2.14})$$

The above differential equation can be easily solved for $M = J_e(W)/J_e(0)$, so for $\alpha_e \neq \alpha_h$, the result of multiplication gain is $M = (\alpha_e - \alpha_h)/\{\alpha_e \exp[(\alpha_e - \alpha_h)W] - \alpha_h\}$, from which, eventually the M can be obtain by

$$M = \frac{1 - k}{\exp[-(1 - k)\alpha_e W] - k} \quad (\text{Equation 2.15})$$

The single-carrier multiplication result for the gain, with its exponential growth, is recovered when $k = 0$. When $k = \infty$, the gain remains unity since only electrons are injected and electron does not multiply. For $k = 1$, (which means $\alpha_e = \alpha_h$ and if assume the electric field across the i-region is uniform or constant) the carriers accelerated in opposite directions will suffer ionization collisions, creating more pairs. In this case the M for $\alpha_e W < 1$, can be define by

$$M = 1 + \alpha_e W + (\alpha_e W)^2 + (\alpha_e W)^3 + \dots + (\alpha_e W)^n + \dots = \frac{1}{1 - \alpha_e W} \quad (\text{Equation 2.16})$$

Avalanche occurs when the current at breakdown goes to infinity ($M \rightarrow \infty$). Therefore, the condition for avalanche is $\alpha_e W = 1$ and M must be obtained directly from main Equation 2.12.

2.4.2 Photocurrent

A total multiplied output current I_{ph} is related to the multiplication gain M by

$$I_{ph} = I_{pr} M \quad (\text{Equation 2.17})$$

Where I_{pr} is the primary un-multiplied photocurrent. Thus, the responsivity of APD can be considered as

$$\mathcal{R} = \left(\frac{\eta q}{h\nu} \right) M \quad (\text{Equation 2.18})$$

$$\mathcal{R} = \left(\frac{\eta q \lambda}{hc} \right) M \quad (\text{Equation 2.19})$$

Where, q is electron charge and η is the quantum efficiency.

2.4.3 Noise in APD

An important consideration in the performance of optical receiver is generation of noise.

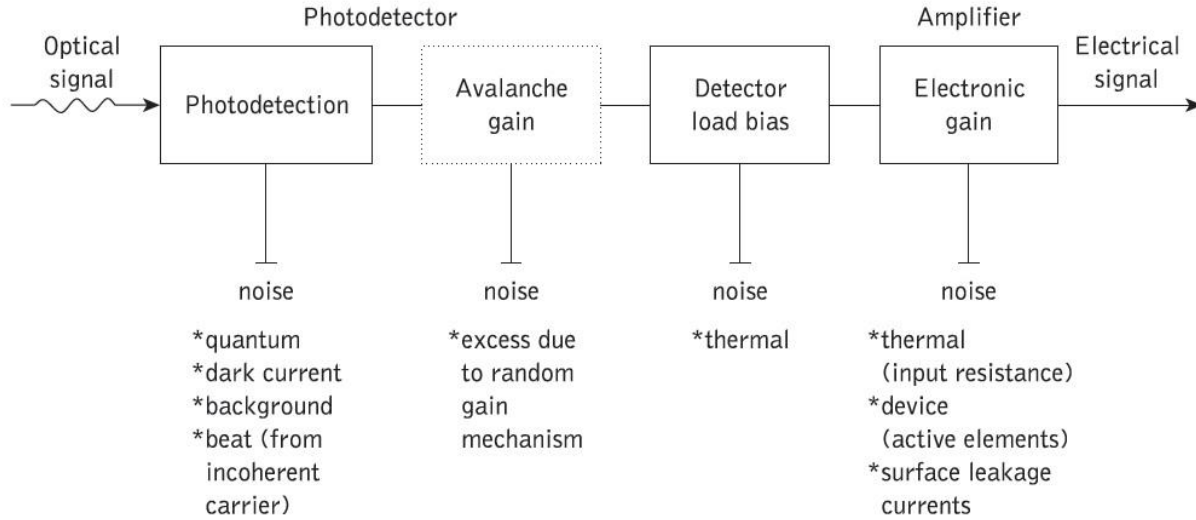


Figure 2.5. Block schematic of various noise sources in the optical receiver [4].

Investigation of APD noise in great details requires considering various type of noise that can possibly be generated by optical receiver. Figure 2.5 shows the various noise sources associated with the optical receiver. Most of these noise sources apply to both types of detector (PIN and APD) [4]. The APD has the most complex noise condition as there is noise generated from random fluctuation of internal gain process.

The first noise term to consider is a dark current of the photodiode which is kind of origin of the other noises as well. Generally, the dark current in photodetectors is related to the saturation current under the reverse bias and is given by

$$I_D = I_{sat} \left(e^{\frac{qV_A}{k_B T}} - 1 \right) \quad \text{(Equation 2.20)}$$

Where, I_{sat} is saturation current under the reverse bias, $K_B=1.38 \times 10^{-23}$ Boltzmann constant and T is temperature.

Dark current and its associated noise is one of the most concerned downward of the photodiodes especially the APDs (since the multiplication process can boost I_D as well). Generally, the following noise currents represent the total noise in a photodiode.

1. Thermal noise: The noise is principally generated by the large dark current of the device and is known as Johnson or Thermal noise and it is originated from the random motion of carriers that contribute to the current. The thermal noise (Johnson) has been formulated [1] and express as

$$I_{Jn} = \sqrt{\frac{4K_BTB}{R_C}} \quad (\text{Equation 2.21})$$

Which B is Bandwidth and R_C is resistance of photo-conductive channel, also known as R_{sh} shunt resistance (in electrical equivalent circuit of photodiode).

2. Background noise: There is always a background radiation in which the detector is placed. Although it has very low intensity (which the magnitude could be as low as Nano or Pico amperes), it will give rise to unwanted photocurrent known as background current (I_B). However, the I_B is more important and applied for atmospheric propagation and it is negligible in optical fiber receiver that uses PIN and APD.
3. Shot noise: The cause of fluctuation in the photodiode carrier concentration is the fluctuation in generation and recombination process known as generation-recombination noise or shot noise which lead to the fluctuation in semiconductor conductivity. The device shot noise determined by

$$I_{sh} = \sqrt{2q(I_P + I_D + I_B)B} \quad (\text{Equation 2.22})$$

As the equation shows the shot noise current is a function of both dark current and photo current statistical fluctuation. By flowing current through the photodiode, the voltage fluctuation (noise) will capture in output.

In the APD however, the multiplication gain must be considered as well since it has amplifier effect on the current and therefore, the equation can be written as

$$I_{sh} = \sqrt{2q(I_P + I_D)BM} \quad (\text{Equation 2.23})$$

APDs have one additional noise factor due to avalanche process known as excess noise. Like any statistical process, there is random fluctuation in the actual distance between successive ionization collisions. These variation, in turn, gives rise to fluctuations in the total number of secondary carriers generated for each primarily carrier injected into the multiplication region. This fluctuation will cause excess noise in the total photocurrent. To minimize avalanche noise, the electron-hole ionization coefficient ratio (k), should be kept as large or as small as possible, by making the avalanche process asymmetrical. In the material such as GaAs and InP, the probability of ionization is nearly identical for both types of carriers, a large density of carriers of both types is generated during avalanche; secondary holes and electrons can generate further carriers. Therefore, for hole injection into the high electric field region the excess noise is given by

$$F_h = M_h \left\{ 1 - \left[1 - \left(\frac{1}{k} \right) \right] \left[\frac{(M_h - 1)}{M_h} \right]^2 \right\} \quad (\text{Equation 2.24})$$

For electron injection, the excess noise factor for electron is given by

$$F_e = M_e \left\{ 1 - (1 - k) \left[\frac{(M_e - 1)}{M_e} \right]^2 \right\} \quad (\text{Equation 2.25})$$

The excess noise factor (F_h and F_e) taking into account the fluctuation in the multiplication process itself. Avalanche noise is minimized by using the material with large ionization coefficient ratio, these kinds of devices can be used at higher gain instead of the detectors fabricated with materials having ionization coefficient close to one.

To summarize what have been discussed, it must be mentioned that the fluctuation of the charge particles due to thermal, background radiation and generation-recombination make the mentioned particles to be always in state of the motion. To distinguish between the input signal and random noise the photodiode must have high signal to noise ratio (SNR) as

$$SNR = \frac{\text{input signal power}}{\text{noise power}}$$

As it has been mentioned earlier, in the case of APD the avalanche process not only enhance the photocurrent, it also increases the magnitude of all noise current. As such, the SNR of avalanche photodiode with its associated noise and multiplication effect is expressed as [2][4]

$$SNR = \frac{I_P^2 M^2}{2q(I_P + I_D)FB + \frac{4k_B T F_n}{R_{eq} M^2}} \quad (\text{Equation 2.26})$$

Where, F_n is amplifier noise factor, and $R_{eq} = \frac{1}{R_{sh}} + \frac{1}{R_s} + \frac{1}{R_L}$

The R_{eq} can be ignored since R_{eq} is a combination of the low resistances

2.4.4 Response time And Bandwidth

Aside from RC effect (which R is junction resistance and C is the junction capacitance), carrier transit time from absorption region to depletion region and diffusion time govern the response time of APD. APDs suffer from two additional limiting parameters. One is multiplication time called avalanche build up time [3]. The second factor is the secondary carriers transit time. Therefore, the response time is given by

$$\tau = \left(\frac{W_d}{v_e} + \frac{W_d}{v_h} \right) + \tau_m \quad (\text{Equation 2.27})$$

Where, W_d is width of absorption region, v_e is saturation velocity of electron, v_h is saturation velocity of hole and τ_m is the multiplication time. Because of the randomness of multiplication process, the multiplication time (τ_m) is random as well. In the special case when the $k = 0$ (no hole multiplication) the maximum value of multiplication time is

$$\tau_m = \left(\frac{W_m}{v_e} + \frac{W_m}{v_h} \right) \quad (\text{Equation 2.28})$$

Where W_m is width of multiplication region. For a large gain, and for electron injection with $0 < k < 1$, the average value of τ_m is obtained by increasing the first term of the Equation 2.28 as follow [3][4]

$$\tau_m \approx \left(\frac{MkW_m}{v_e} + \frac{W_m}{v_h} \right) \quad (\text{Equation 2.29})$$

When the gain is high enough the bandwidth and avalanche build up time are inversely proportional. Since the gain and avalanche build up time are directly proportional, thus the gain-bandwidth (GBW) product is function of the gain.

2.5 APD Design

This section contains the discussion of the three type of APDs design structure, the thickness of absorption layer width and multiplication layer width as well as the structure and material parameters.

2.5.1 Separate Absorption and Multiplication APD

Like any other photodiode, an APD structure should be designed with two important requirements. First, high photo absorption. Second, the multiplication region must be sufficiently thin to reduce (or avoid) the possibility of localized uncontrolled avalanche process or avalanche instabilities, being produced by high electric field. Thin region can lead to greater electric field uniformity. These two contradictory requirements call for APD design, which has separate absorption and multiplication region. This kind of structure is known as Separate Absorption and Multiplication APD (SAM APD). The operation of the SAM avalanche photodiode can be easily understood by assuming $k \approx 0$. Photons are absorbed in large intrinsic and lowly doped region. The generated carriers drift across this region due to moderate electric field, and then enter to the multiplication layer with the strong electric field where the avalanche multiplication process occurs [3][4]. The SAM APD structure illustrated in Figure 2.6 accomplishes this. (In this structure the p^+ region is highly doped while, the gain and absorption regions are lightly doped.)

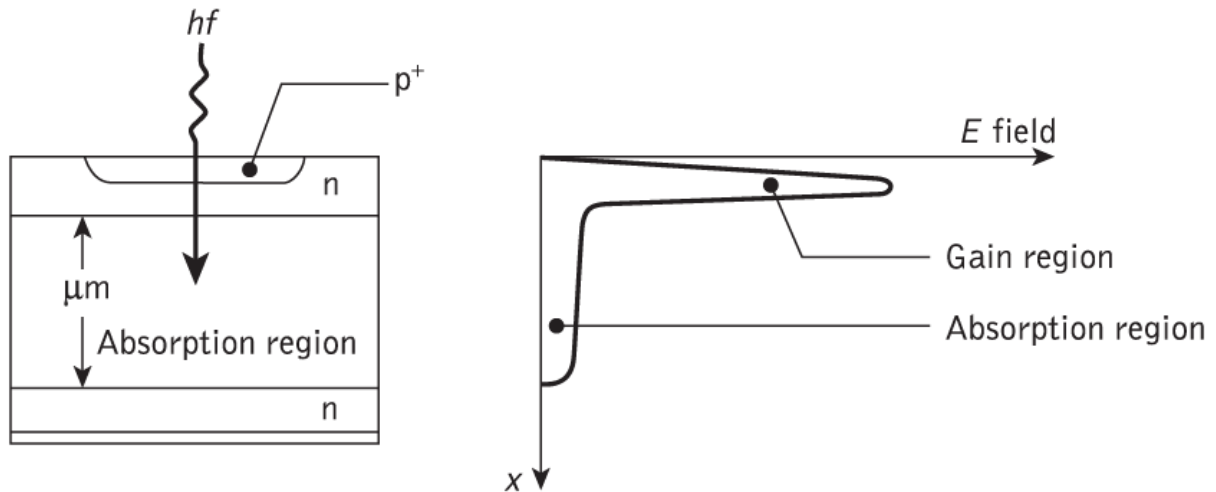


Figure 2.6. SAM p+-n-n APD structure [4].

Photo absorption occurs in the wide lightly doped (intrinsic) absorption region. Generated carriers drift via the absorption region into a thin p^+n junction, where they experience a sufficiently strong electric field to cause the avalanche multiplication. The reverse bias applied across the device is large enough for depletion layer to reach through the multiplication and absorption regions into the p^+ contact layer. The reach through APD structure ensures that the avalanche process is primarily due to the carriers with higher impact ionization coefficient (electron in case of Si APD or holes in case of InP APD). Thus, the avalanching time decreases and therefore, the response of device is faster [3]. It is obvious that the choice of material for an APD is dictated by the application. Figure 2.7 shows the Responsivity versus Wavelength for several materials. As it illustrated, Silicon is the most suitable for the application with absorption range of 0.6 μm to 0.9 μm wavelength. And for the fiber optic communication, the InGaAs is the material of choice since it has the bandgap of 0.78 eV, which corresponds to a wavelength of 1.5 μm . However, the homojunction diodes made of these low bandgap materials have high reverse leakage current at high voltage due to band to band tunneling.

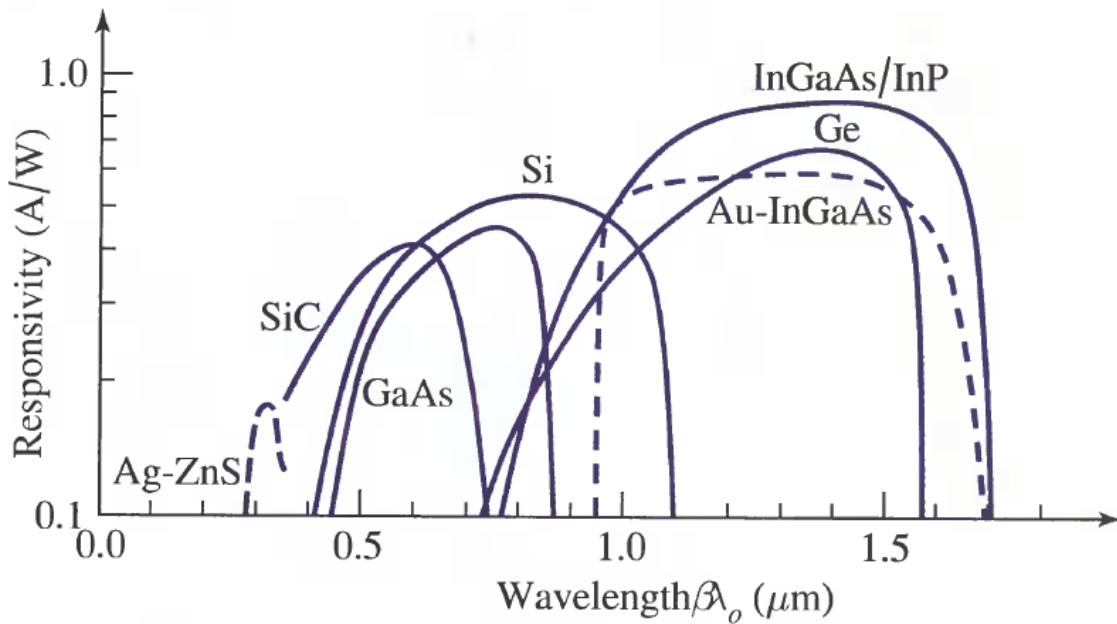


Figure 2.7. Responsivity \mathcal{R} versus wavelength λ for number of photodiodes [3].

The leakage current can be reduced by incorporating the high electric field avalanche multiplication region of the device in large bandgap material.

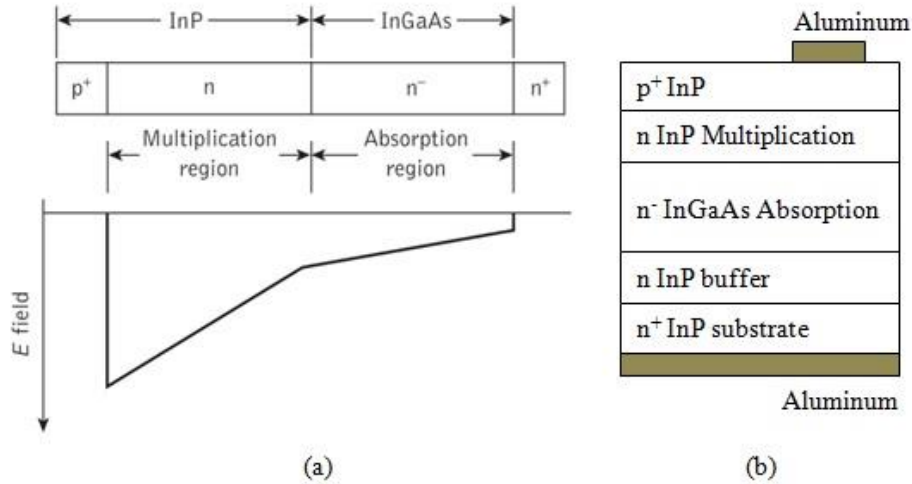


Figure 2.8. Separate absorption and multiplication (SAM) APD. (a) Layer composition and electric field profile (b) cross section of SAM APD [4].

These considerations lead to InGaAs/InP SAM APD as illustrated in Figure 2.8. The structure combines low leakage current, due to the junction being placed in the large bandgap material such as InP, with sensitivity at longer wavelengths provided by the low bandgap absorption region such as InGaAs.

The issue with SAM APD, however, is that holes can accumulate (trapping) at the valence band discontinuity at the InGaAs/InP heterojunction as shown in Figure 2.9 (a) and therefore increase the response time [12]. To resolve this problem, Separate Absorption Graded and Multiplication (SAGM) APD has been presented. This structure, is slightly different than SAM APD. A graded bandgap quaternary InGaAsP layer is inserted between absorption layer (InGaAs) and multiplication layer (InP) to alleviate this issue (Figure 2.9 (b))[4]. The thin layer of InGaAsP ensures a moderate low electric field in absorption region. To ensure low noise operation, in the designing of these devices, it is important to be sure that first, all the absorption occurs only in the absorption region, second, the carrier type, which has higher impact ionization coefficient in the multiplication region, is injected into it. The SAGM APD structure further developed by adding the one more layer between multiplication and grading layers to regulate the electric field

distribution in multiplication and absorption layers. As such, the final structure as shown in figure 2.9 (c) called SAGCM InGaAs/InP APD.

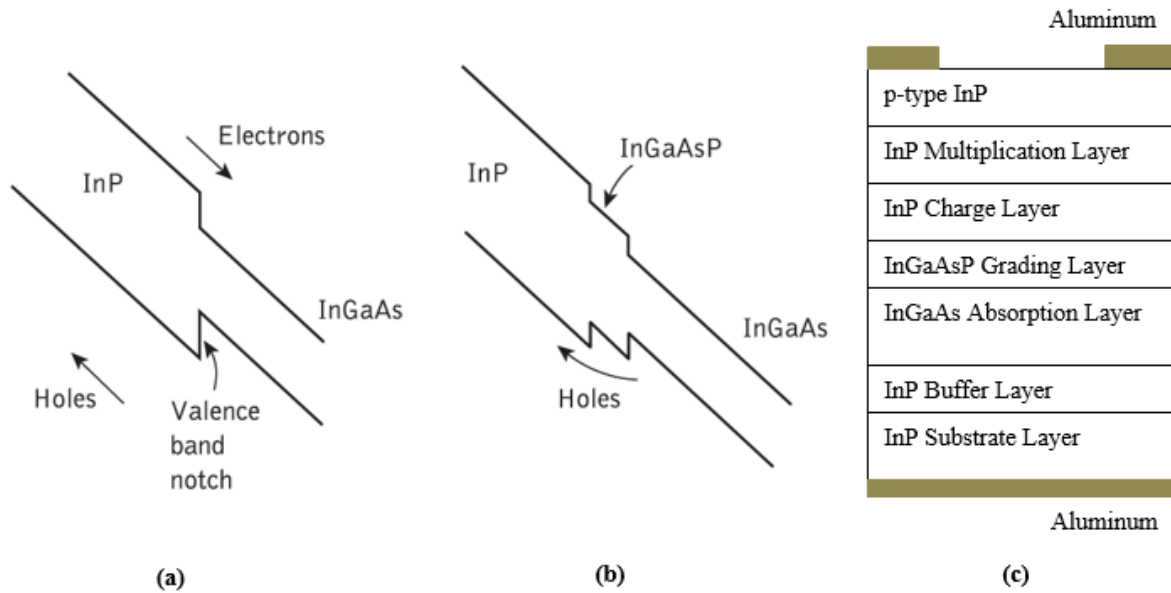


Figure 2.9. Energy band diagrams for SAM and SAGM APDs [4][12].

2.5.2 Absorption Layer Width and Multiplication layer Width

The two important performance parameters in APDs are the punch-through voltage (V_{p-t}) and breakdown voltage (V_b). The punch-through voltage define as the voltage at which the depletion region expand to the absorption layer. And the voltage point where the APD gain goes to infinity (avalanche breakdown occur) consider as breakdown voltage [5].

In the avalanche photodiode the thickness of absorption layer or Absorption Layer Width (ALW) dominate the photocurrent, dark current, and speed of APD since all carriers initially generated in this layer and the carriers transmission time also depends on this layer thickness in which the larger ALW lead to higher carriers transmission time. On the other hand, the thickness of multiplication or Multiplication Layer Width (MLW), is the key parameter of the breakdown voltage and the position at which avalanche process is going to occur. By design, this layer supports a high electric field region where the photogeneration and thermally excited carriers (holes) drifting across the depleted charge layer that can undergo avalanche multiplication [6]. The MLW directly controls

the magnitude of the electric field and thus, From the Gauss law and its general relation with voltage (V), it is proven [47] that can define the electric field (E) for the two distanced (d) surfaces by the following equation

$$E = \frac{V}{d} \quad \text{(Equation 2.30)}$$

This equation can use to explain the electric field in the APD by replacing d with layer width (in this case MLW). Therefore, for the small MLW, electric field in the multiplication layer increases (and that is why in thin MLW, although, the travel area is small, carriers can gain enough energy to initiate impact ionization) [46]. And for the large MLW electric field decreases. However, for large MLW the voltage has to be lager to maintain the electric field strengths (therefore the carriers are able to travel longer distance with a lower electric field for large MLW) [46].

2.5.3 Structure and material Parameters

Table 2.1 presents structures of a few InP-based APDs [5][6][8]. As it is illustrated in designing an APD, the 2-3.3 μm thick absorption region is undoped. The graded layer (0.09-0.6 μm) and the multiplication layer (0.5-1.5 μm) are doped to maximum $7 \times 10^{16} \text{ cm}^{-3}$. The multiplication layer thickness directly controls the electric filed magnitude and therefore, by an exponential relation, the rate of impact ionization. Moreover, the thinnest possible of this layer will lead to the shortest time of avalanche build-up process [6]. The p^+ -InP layer can be thin and doped to $10^{17} - 10^{18} \text{ cm}^{-3}$.

Table 2.1: The thicknesses and their Doping Concentrations of a few InGaAs/InP APDs.

| Layers specification | Absorption region In _{0.53} Ga _{0.47} As | Graded region InGaAsP | Multiplication region i-InP | p ⁺ -InP | References |
|----------------------------|---|--------------------------|--------------------------------|---------------------|------------|
| Thickness (μm) | 2.83 | 0.012×5 | 0.59 | 2.77 | |
| Doping (cm ⁻¹) | 1×10 ¹⁸ | 1×10 ¹⁶ | 1×10 ¹⁵ | 4×10 ¹⁷ | [5] |
| Thickness (μm) | 3.3 | 0.09 | 0.3 | 2.2 | |
| Doping (cm ⁻¹) | 7×10 ¹⁴ | 7×10 ¹⁶ | 7×10 ¹⁴ | 7×10 ¹⁸ | [6] |
| Thickness (μm) | 2.8 | 0.012×5 | 0.5 | 2.0 | |
| Doping (cm ⁻¹) | 1×10 ¹⁵ | 2×10 ¹⁶ | 1×10 ¹⁵ | 1×10 ¹⁸ | [8] |

For high speed operations of these devices it is desirable to deplete all or most of the absorption region. Otherwise, carrier transit is dominated by the slow diffusion of carriers [2].

The material parameters also play a significant role in design and performance of an APD. The thickness of material required in the absorption region, is depending on the absorption coefficient α which is one of the material characteristics. Figure 2.10 shows the absorption coefficient versus wavelength for different semiconductor materials. As it illustrated for the longer wavelengths (1.55 μm) the InGaAs has larger α which can lead to design sufficiently thin absorption layer.

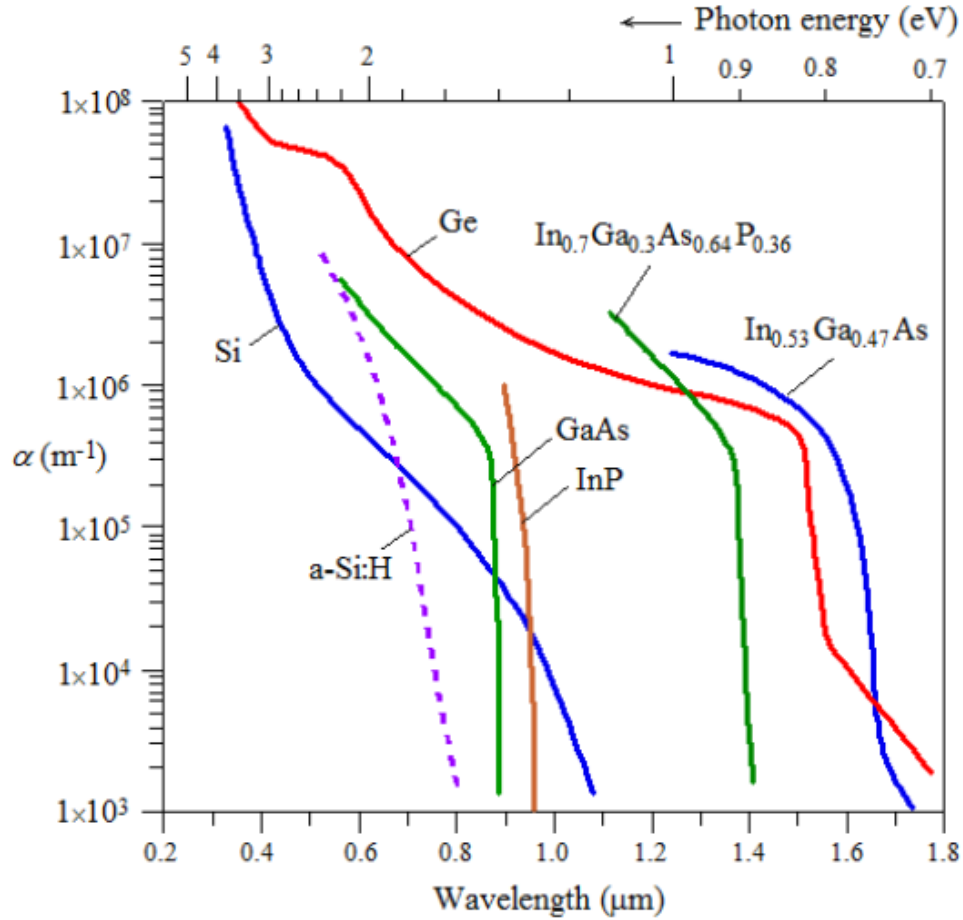


Figure 2.10. Absorption coefficient versus Wavelength for several material [1].

One of the effective parameters that needs to be considered is the carrier lifetime, which dramatically affects the dark current at the punch-through voltage [8]. Table 2.2 shows the Shockley-Hall-Reed (SHR) lifetime for the conventional InGaAs/InP APDs. The SRH lifetime for InP is $10^{-9} \sim 10^{-12}$. However, the practical experiment showed that 10^{-9} is much better value in case of fabrication. InGaAs on the other hand, has minimum SRH of 10^{-4} .

Table 2.2: SRH lifetime value.

| Material | Electron SRH Lifetime (s) | Holes SRH Lifetime (s) | Reference |
|----------|------------------------------|---------------------------|-----------|
| InP | 1×10^{-9} | 1×10^{-9} | [5] |
| InGaAs | 1×10^{-6} | 1×10^{-6} | |
| InP | 1×10^{-9} | 1×10^{-9} | [6] |
| InGaAs | 2.2×10^{-4} | 2.2×10^{-4} | |
| InP | 6.0×10^{-12} | 6.0×10^{-12} | [34] |
| InGaAs | 8.0×10^{-8} | 8.0×10^{-8} | |

2.6 Simulation

The need for more accurate and more complete simulation techniques was first considered through transistor development. As the development of the bipolar junction transistor (BJT) and later MOS technologies became smaller the need for process and device modeling became more important. Initially, the advancement of Technology Computer Aided Design (TCAD) software was driven by the need for process development simulation in research environments [43]. The history of TCAD software development started at Stanford University with the development of the Stanford University Process Modeling (SUPREM) [44]. Newer versions of the original SUPREM have been implemented in the most widely used simulation platforms of today.

Simulation software for industry-standard devices can be used to predict the electrical, optical and thermal characteristics of semiconductor devices and to model a wide range of devices in one, two, and three dimensions. The simulation software module incorporates the most advanced commercial models available to simulate and optimize the device design for optimum performance without the need of a rung, which avoids costly experimentation. Technology Modeling Associates, Inc. (TMA) was the first company to commercialize a version SUPREM (TMA was later acquired by Avanti and then Synopsys). Later, Silvaco produced a product named ATHENA based on SUPREM. More recently Integrated Systems Engineering (ISE) came out with their own process simulator named DIOS (ISE was later acquired by Synopsys as well). Synopsys and

Silvaco are now, by far, the two leading providers of process simulation software today. Both companies also provide a line of device simulators that work in harmony with their process simulation software.

Silvaco and Synopsys provide server-based simulation platforms which capable to run on Linux operating system (Redhat to be precise) with absolutely no limitation in terms of running desirable modules. There is a few editions of these simulation programs for Windows operation system (OS) as well. However, they (especially Silvaco) have simulation limits on Windows OS, since the platform does not support all modules and subprograms on Windows OS. The simulation capability of Silvaco platform and Synopsys platform (Sentaurus TCAD) is the same in 1D, 2D and 3D simulation while they have different integrated development environment (IDE). They both are powerful enough to enable the device engineers [34][44]

1. To predict the electrical, optical and thermal characteristics of semiconductor devices by precise simulation without having to create the actual device.
2. To have strong scalability based on advanced C++ software architecture and mature and efficient numerical analysis algorithms
3. To have extensible platform to analyze DC, AC, and time domain responses for all semiconductor-based technologies
4. To optimization devices and finding of ideal structural parameters without the need to create actual devices.
5. To study breakdown and failure mechanisms, such as leakage current paths and hot carrier effects.
6. To prepare data for generation of small models to analyze circuit design prior to flow

In some APD investigations [28][32][33], Silvaco has been used for 2D or 3D design simulation and numerical calculations. And in some others [5][8][15] Sentaurus has been chosen. In all of those investigations, Silvaco and Sentaurus have successfully achieved precise and reliable results. Since the capability of both simulation software are the same, the choice of employment for one

of these two, is mainly based on which one is commercially available or which one the engineers find easier to start with.

2.6.1 Simulation of APD

The simulation of APD requires the simulator program, which is capable of specifying the wide range of material and combination of them such as binary, ternary and quaternary compound. In addition, it must have a variety of methods to simulate the light propagation as similar to the real light source. Furthermore, the simulator must include with the wide range of integrated numerical parameters, methods, and optical index profile as well as the models and programs that capable of simulate, define heterojunction structures, and can predict the DC and AC behavior of the defined structure. It has been briefly mentioned in the previous section that there are two main simulation programs (Silvaco and Sentaurus) that powerful enough to simulate the avalanche photodiode. In as such in this work the Silvaco has been adapted to simulate the SAGCM InGaAs/InP APD. Three main modules and program that have been taken huge advantages from in this simulation work are as follow [34]:

- a. Atlas: it is a physical based device simulator. Which is able to predict the electrical behavior of defined semiconductor structures and provides insight into the internal physical mechanisms associated with device operation. Atlas, also is able to be use as independent simulator or as a core tool in Silvaco's Virtual Wafer Fab simulation environment [34].
- b. Blaze: It is a general purpose device simulator for III-V, II-VI materials, and devices with position dependent band structure as like the heterojunction devices. Blaze accounts for the effects of position-dependent band structure by modifications to the charge transport equations and Poisson's equation. Blaze is applicable to a broad range of devices such as LEDs, lasers, heterojunction photodetectors (e.g., APDs, solar cells) and heterojunction diodes.
- c. Luminous: It is a general purpose light propagation and absorption program integrated into the Atlas framework. This program is able to calculate optical intensity profiles within the semiconductor device and then it will be converted into photo-generation rates.

More details and example of the APD is simulated and which methods have been used will be discussed in next chapter.

CHAPTER 3

METHODOLOGY

3.1 Device Simulation

The methods in which a simulation platform arrives at a solution file are many. Through the years there have been numerous models and methods used to outline semiconductor device structure. Furthermore, some models and numerical methods can be combined with each other while others might not be compatible. Because of this, there are multiple ways that a problem can be solved using simulation software.

For the simulations involving the APD and other typical device simulations, there are two main factors that must be solved. Firstly, it is the carrier transport equations which describe and govern how charge flows in the device. The second is the electric fields in the device. These two factors are very much related to each other. The dynamics of charge flow are determined by electric fields and the electric fields dynamically change as mobile carries flow. Since these two factors are dependent on one another, they must be solved simultaneously in some fashion. The solving of these two factors can be extremely taxing, computationally, if approximations or assumptions are not made.

Many research and development have gone into the mathematics and device structure to derive the fundamental equations that are used to evaluate potential and charge on the various levels needed for semiconductor device simulation. These equations all find their origin in Maxwell's laws. Maxwell's laws [36] in their differential form are as follow:

$$\nabla E = \frac{\rho}{\epsilon_0} \quad (\text{Equation 3.1})$$

$$\nabla B = 0 \quad (\text{Equation 3.2})$$

$$\nabla \times E = -\frac{\partial B}{\partial t} \quad (\text{Equation 3.3})$$

$$\nabla \times B = \mu_o J + \mu_o \epsilon_0 \frac{\partial E}{\partial t} \quad (\text{Equation 3.4})$$

From these laws, the fundamental equations that link electric field to carrier densities in simulations were formed. The main equations used in typical device simulation, as derived from Maxwell's laws, are Poisson's Equation, the continuity equations and the carrier transport equations. These equations and their purposes in device structure and analysis will be discussed briefly. Poisson's Equation [40] in one of its forms is shown by

$$\nabla^2 V = -\nabla E = -\frac{\rho}{\epsilon_s} = \frac{q(n - p + N_A - N_D)}{\epsilon_s} \quad (\text{Equation 3.5})$$

It relates variations in electrostatic potential to local charge densities. It is typically derived from Gauss' law (Equation 4.1). Gauss' Law and the Poisson equation are basically different forms of the same equation which relates the distribution of electric charge to the electric field. Poisson's equation becomes necessary when evaluating how charge density distributions affect electric fields within a depletion layer and vice versa. The continuity equations are time dependent equations dealing with net charges. They describe the net charge of a carrier concentration by relating the generation and recombination rates and the current densities over time. One way to express the continuity equations for electrons and holes are [40]

$$\frac{\partial n}{\partial t} = G_n - U_n + \frac{1}{q}(\nabla J_n) \quad (\text{Equation 3.6})$$

$$\frac{\partial p}{\partial t} = G_p - U_p + \frac{1}{q}(\nabla J_p) \quad (\text{Equation 3.7})$$

Where, equations G_n and G_p are the carrier generation rates for electrons and holes respectively. While, U_n and U_p are the recombination rates.

These rates are affected by things such as the type of semiconductor material, impurity concentration, defects, temperature, impact ionization and other factors such as optical exposure.

The transport equations are the equations that describe the mobility, drift and diffusion of carriers (for electrons and holes) in the presence of an electric field in space by

$$J_n = q\mu_n nE + qD_n \nabla n = \mu_n n \nabla E_{Fn} \quad (\text{Equation 3.8})$$

$$J_p = q\mu_p nE + qD_p \nabla n = \mu_p n \nabla E_{Fp} \quad (\text{Equation 3.9})$$

In these two equations, the carrier mobility for electrons and holes is represented by μ_n and μ_p , the diffusion length for the material and conditions for the same carriers are D_n and D_p and the electron and hole Fermi levels are E_{Fn} and E_{Fp} . Both Equations 3-8 and 3-9 provide the foundation for semiconductor device operation. They are the framework for the device simulation platforms. They define how factors such as temperature dependence, optical generation, impact ionization, static and dynamic potentials, doping levels and much more affect the device operation.

3.2 Choice of Simulation Models

As devices became more technologically advance, (complicated and exponentially smaller in size) the assumptions and approximations that have been used classically, were no longer sufficient. Furthermore, as the devices evolved so did the numerical methods used in simulation. One of the most useful equations when analyzing and modeling semiconductor devices and carrier transport is Boltzmann's Transport Equation [35][38] which is probabilistic in nature. It is often referred to as semi-classical because it delves into the quantum theory of Heisenberg's uncertainty principle which states that only the likelihood or approximate position and momentum of a particle can both be known in a given moment. For this reason Boltzmann's Transport equation is strongly based on probability theory to estimate position and momentum in time given complex scattering functions. The simple general form of Boltzmann's Transport equation [40] can be express by

$$f(x, p, t) = \frac{\partial f}{\partial t} + v \cdot \nabla_x f + E \cdot \nabla_p f \quad (\text{Equation 3.10})$$

The details of the function are not necessarily important for the scope of this discussion. It should be noted that it is almost an impossibly difficult function to solve when applied to particles in semiconductor devices. This is because location and momentum exist in three dimensions each (assuming no simplification or assumptions) and time in one dimension [40].

The most frequent model used, base of these assumptions and simplifications, is the drift-diffusion model [33][34]. The drift-diffusion model is used when analyzing devices that are on the order of a half micron or bigger in feature sizes. For many practical devices this is sufficient. When modeling the APD, versions of the drift-diffusion model are used almost exclusively because the assumptions made to simplify Boltzmann's Transport equation into the drift-diffusion model are applicable. These assumptions and approximations tend to rely on classical analysis and away from quantum mechanics. In typical carrier transport this is often sufficient. However, once the device size gets below this point then quantum-like effects begin to play a significant role in the way the device operates [40]. When this occurs, less simplified versions of the drift-diffusion model can often be implemented. Later, for device sizes smaller than a half micron, many device simulation platforms often use a version of the hydrodynamic model which takes things like hot carriers and other quantum effects into more careful consideration. If the devices get even smaller and device sizes approach below 100 nm and into the ones of nanometers then it becomes necessary to utilize particle based simulations and model like the Green's function or the Schrödinger equation [39]. For modeling and predicting performance for micro-scale devices such as photodiodes and the APD, the drift-diffusion model is typically sufficient. Additional considerations need to be taken into account for impact ionization and other effects but in this device size range the assumptions used are sufficiently accurate. With the introduction of hot carriers, tunneling, impact ionization or other quantum or quantum-like effects other equations must be added to the drift-diffusion model to make it complete. Because the drift-diffusion model is used in the Silvaco platform which, in turn, is used in simulating the APD, its application and Silvaco will be discussed in greater detail in the next section.

3.3 Device Simulation in Silvaco

Silvaco is the platform chosen to model the InGaAs/InP APD. Silvaco comes with a broad range of capabilities. It provides quite a set of physical models including:

1. DC, AC small-signal, and full time-dependency.
2. Drift-diffusion transport models.
3. Energy equilibrium and Hydrodynamic transport models.
4. Lattice heating and heat sinks.
5. Graded and abrupt heterojunction.
6. Optoelectronic interactions with general ray tracing.
7. Amorphous and polycrystalline materials.
8. General circuit environments.
9. Stimulated emission and radiation
10. Fermi-Dirac and Boltzmann statistics.
11. Advanced mobility models.
12. Heavy doping effects.
13. Full acceptor and donor trap dynamics
14. Ohmic, Schottky, and insulating contacts.
15. SRH, radiative, Auger, and surface recombination.
16. Impact ionization (local and non-local).
17. Floating gates.
18. Band-to-band and Fowler-Nordheim tunneling.
19. Hot carrier injection.
20. Quantum transport models
21. Thermionic emission currents [34].

Silvaco is a professional platform capable of powerful numerical methods and a broad range of models that can be used to accurately describe many semiconductor devices. In device simulations, many models are used. As discussed earlier, the default model used by Silvaco in device simulation

is the drift-diffusion model. Also mentioned in the previous section, the drift-diffusion model is a simplification of the Boltzmann Transport Equation. The simplification is made by making certain assumptions based upon the device setup. These assumptions and simplifications may vary yielding different versions of the drift-diffusion model. Some of the typical assumptions used in the derivation are things like parabolic-like bands, steady-state conditions, one to two dimensional space, classical particle theory, discrete device dimensions, the absence of temperature gradients, low electric fields and so forth. No matter the assumptions and simplifications the drift-diffusion model is always based on Equations 3.8-3.9 (Poisson Equation, Continuity Equations, and Carrier Transport Equations) in one form or another. Other models and corrections can be added to the base model to account for device specific phenomenon and this is usually the case. When additional models are included in a simulation other equations are added that must be solved simultaneously with Equations 3.5-3.9. Not all of the models are compatible with each other and will cause run-time errors or convergence problems when improperly combined.

The basic process to obtain a solution set is the same for the different methods used. First the device is outlined and a mesh is defined (either by a process simulation or through direct specification). The mesh is a series of nodes and quadrants that are used when solving the coupled set of equations. After the mesh and geometries of the device to be simulated are set, the materials and doping are assigned within that geometry. Then voltages and currents are applied giving rise to electric fields and current densities. The dynamics of the electric fields and current density through the device are calculated through a process of iterated solutions to a discretized version of the continuous device. The discrete sections are defined in the geometry mesh setup and are very important to the accuracy and efficiency in obtaining a solution. An example will be given in a future section.

The system is solved by using an iterative process that makes estimates to the solution set and refines them in each iteration. Each iteration through the solving method is based upon the last iteration and is started by an initial guess at the solution set. The iterations get closer and closer to a solution of the set of equations determined in the model. All of the equations must have an agreeable solution to the device setup. If the device setup and initial guess were sufficiently well described the simulations will converge on a solution set and the data can be analyzed. There are

preset convergence criteria and the iterations will continue until either the criteria are met or it becomes apparent that they will not be met (divergence).

Different methods can be used in the iterative process to analyze the system of equations used. When choosing between the different methods, the choice is usually based up the likelihood of convergence given the setup and method chosen and how quickly an accurate solution set can be obtained. Accuracy, or how well a model compares to real life, is very desirable but the trade-off between accuracy and simulation time needs to be taken into consideration. The device mesh and numerical methods chosen should be efficient and be able to handle a wide variety of structures. High accuracy requires a fine mesh that can resolve all significant features of the solution. High efficiency requires a coarse mesh that minimizes the total number of nodes. This trade-off between accuracy and numerical efficiency is frequently a problem.

In Silvaco there are three types of numerical methods that can be applied to a chosen model. These are the Gummel, Newton, and Block methods [34]. These methods are different approaches to solving the dynamic system of equations set out by the model that describe and predict the device operation.

3.4 Gummel method

The Gummel method solves the system of equations by solving them sequentially as opposed to simultaneously [34]. This is typically done by solving for Poisson's equation given the initial conditions. This is done for each mesh triangulation and the boundaries are set equal for adjoining triangulations. Using the potential obtained from this solution the continuity equations are solved followed by the current transport equations. This concludes a typical iterative step which now cycles back on itself solving for Poisson's equation using the current densities and quasi-Fermi levels obtained from the solution to the other equations. This process is repeated until the convergence restraints are met. Convergence is checked every iteration by algebraically positioning the terms on the same side of all the equations and substituting the iterative values in as the variables. Convergence is met when the residuals are smaller than the set tolerance. The rate of obtaining a converging solution in the Gummel method is based upon the coupling between the

equations. If there is little coupling the convergence is reached much quicker. Because this is often not the case the Gummel method usually converges relatively slowly.

3.5 Newton method

The Newton method solves the equations simultaneously as opposed to sequentially [34]. Thus, each iteration in this method solves a linearized version of the entire system of equations. Because of the complexity of this problem (solving a system of equations as opposed to a single equation) each iteration takes significantly longer than the Gummel method. On the other hand, the solution is often converged upon much more quickly given sufficiently accurate initial guesses to the system. As a result of this, the Newton method becomes much more dependent on accurate initial guessing techniques than the Gummel. The Newton method is the preferred method for systems where an accurate initial guess is possible. It is also preferred when the biasing of the system is larger. As the system biasing increases the coupling between the electric fields and the current densities increases. With an increased relationship between current density and electric field the Gummel method becomes quite longtime to obtaining convergence. For most systems the Newton method is the preferred method and as such is the default numerical method technique for Silvaco simulations of the APD.

3.6 Block method

The Block method, in some point, can be thought of as a combination of the Gummel and Newton methods [34]. The Block methods used by Silvaco go through iterations that solve subgroups of equations simultaneously while stepping through these subgroups sequentially. This makes it possible to incorporate more models in the simulation. These models can be approached separately and then combined. Often, this means Newton's method is used to calculate and update the potential and carrier concentrations. Then the Gummel method is used to analyze additional models that are incorporated into the system (the models like, lattice heating, tunneling etc.). Note that the Newton and Gummel methods are both capable of handling additional models as well. But not all models and methods are compatible.

3.7 Silvaco ATLAS

As mentioned in the previous section, all of analyses of the physics behind the operation of the APD have been done using the Silvaco platform. Silvaco is made up of a group of applications that are made to operate together in harmony. Figure 3.1 illustrates the main applications in the Silvaco platform and how they interact [34]. ATHENA is the process simulator.

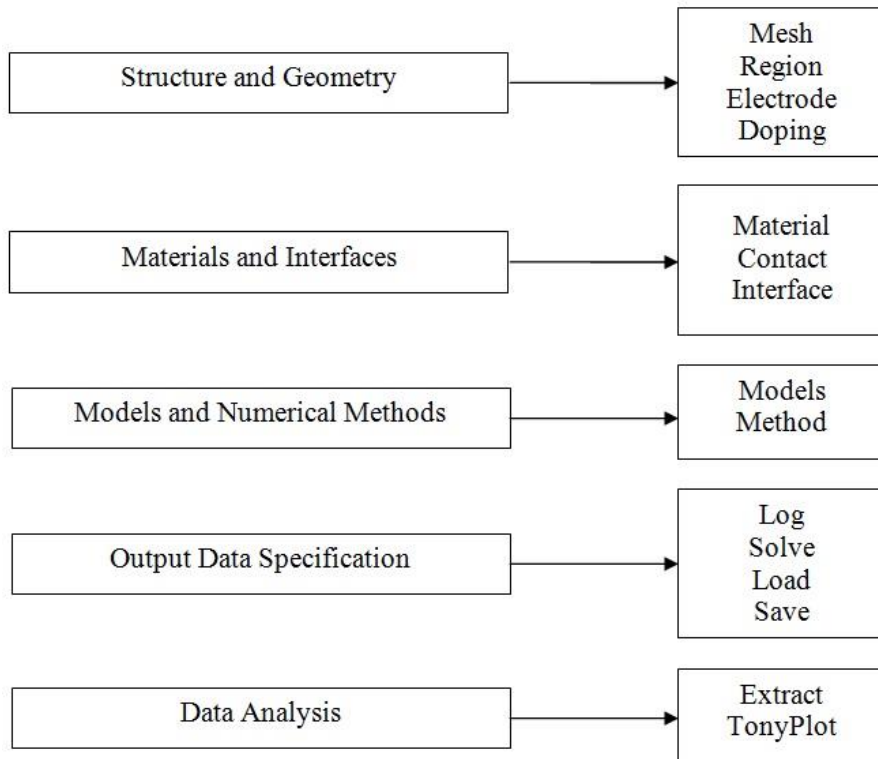


Figure 3.1. The right hand side of the arrows shows the types of commands for process simulation. The left hand side shows the corresponding commands used in the Silvaco platform.

The structure files produced by ATHENA can be directly input into ATLAS for device simulations. If desired, Deckbuild can be used to create a command file independent of a process simulator which can be used by ATLAS for device simulation. In this case, the structure and material definitions are specified in the Deckbuild runtime environment which will be explained

shortly. Once a device has been designed using either ATHENA or Deckbuild, Atlas is used for the device simulation and integration into theoretical systems. During the device simulation, numerous effect are being monitored and recorded as voltages and currents are applied to the device and specified electrodes. ATLAS keeps track of parameters such as mobility, carrier concentration, electric field, recombination, generation, energy levels and much more. Some of this data can be observed real-time via the runtime output. All of the data is output into a series of log and structure files that can be analyzed and observed in the Tonyplot user interface [34]. Once a device has been deemed operable it can be packaged and exported to Silvaco’s spice (discrete device level) simulator interface and inserted into a circuit system. This interface, known as Mixedmode, allows for DC, AC and transient responses to be done on circuit systems with the packaged device integrated seamlessly inside.

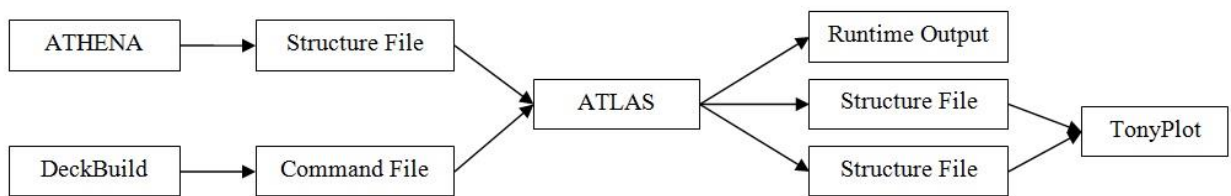


Figure 3.2. Flowchart illustrating the main modules for data analysis and display.

Athena, the process simulator, can be used to accurately model fabrication steps [33]. Through proper setup of the simulation diffusion lengths, an oxide growth, depositions, etches and much more can be simulated with extensive control of the theoretical environment. The setup for a process simulation in Athena is generated in Deckbuild.

3.8 Deckbuild

In Deckbuild commands are outlined to specify the geometries, resolution, and physical factors that a semiconductor material encounters in the fabrication process. Control over semiconductor materials, temperatures, timelines, chemical exposures, impurities, etc., are taken into consideration during these fabrication sessions. As stated earlier, Deckbuild is used to create a

command file for Athena process simulations or Atlas (for device simulations without doing a process simulation previously). In the Deckbuild runtime interface the structure and geometry, materials and interfaces, models and numerical methods, and output data specification are outlined.

Table 3.1: Basic Atlas commands and brief description.

| Command | Description |
|-----------|--|
| Mesh | Sets the resolution for the discretization of the device during simulation. |
| Region | Specifies the different material region in the devices geometry. |
| Electrode | Specifies locations where voltages and currents can be applied. |
| Doping | Sets the doping levels, type, junction depth, etc. |
| Material | Used to assign a material type to each REGION |
| Models | Determines which models will be used to evaluate the carrier densities, carrier transport, and electric fields in the system |
| Contact | Define the type of metal/work function for each specified ELECTRODE. |
| Beam | Define and specify a light source for simulations with an optical source. |
| Method | Specify the numerical methods used in evaluating the chosen models. |
| Log | Output command for applied conditions. Produces a .log file which can be evaluated using TONYPLOT. |
| Solve | Used to apply/change the voltage or current at a specified ELECTRODE. |
| Load | Import a file from ATHENA. |
| Save | Save a design to be exported to MIXEDMODE or TONYPLOT. |
| Extract | Specify specific parameters (aside from the default) that need to be evaluated during runtime. |
| Tonyplot | Open TONYPLOT and evaluate a saved file. |

These parameters can be used to specify device and material characteristics such as carrier mobility, recombination, generation and other effects. After the device has been setup and the models chosen voltages and currents can be applied to the metal contacts for single device DC, AC and transient testing. During the running process the current and voltage can be monitored in Deckbuild as well as the convergence of the overall model. The results are output to Tonyplot in the form of a data curves as well as a cross sections of the device for further analysis and

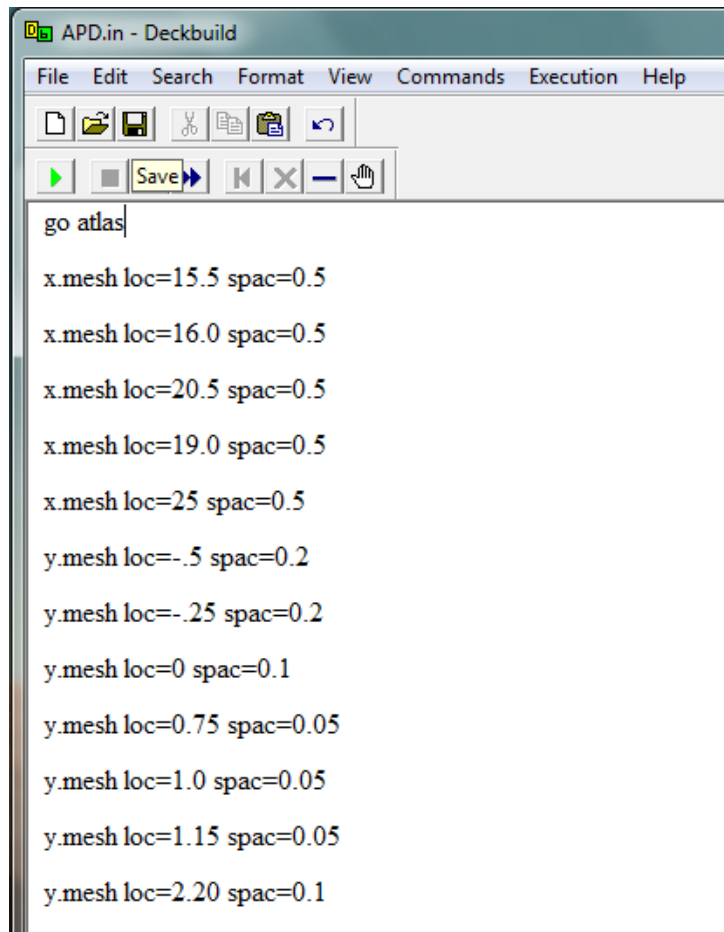
manipulation. The results can also be extracted and exported for analysis in other mediums. Being able to analyze variations to currents, voltages, geometries, doping levels, temperatures and other factors was absolutely necessary during the development of the APD. Analyzing the effects of these changes through traditional fabrication and testing techniques would prove costly and time consuming. Having complete control over the devices structure with predictive results through Silvaco made testing the latest theories and queries possible. The process to set up a simulation using Deckbuild is rather straight forward for most basic devices. The first thing that needs to be done is to understand the statements that are used to define a device's geometry and the parameters that simulate the fields and current densities through the device. A more in-depth look at some of the ATLAS statements can be seen in Table 3.1 [34].

3.9 Basic Device Simulation

The following section will walk through basic setups of construction layout for device simulation in Silvaco.

3.9.1 Mesh Construction

The first thing that needs to be done when setting up a simulation is to specify a MESH. The mesh can either be setup in cylindrical coordinates or in rectangular coordinates. The following is an example of a mesh setup in rectangular coordinates. Once the type of mesh is specified then the locations and spacing are setup. (The simplest way to define locations and spacing of the Mesh is to use mesh auto command follow by only specifying of total x-axis boundary and spacing [34]) For a rectangular mesh this is done by specifying the location of the changes in the mesh spacing starting at the smallest x coordinate in the design (this is usually at $x=0$ but it can be a negative value if desired). After specifying the mesh in the x direction, the y direction is specified in the same way (starting from smallest and going to largest coordinate). The x.mesh and y.mesh commands are used for this process. The mesh used in this example is shown in the Figure 3.3.

The image shows a screenshot of a software interface titled "APD.in - Deckbuild". The interface has a menu bar with "File", "Edit", "Search", "Format", "View", "Commands", "Execution", and "Help". Below the menu bar is a toolbar with icons for file operations (new, open, save, copy, paste, undo) and a "Save" button. The main text area contains the following commands:

```
go atlas  
x.mesh loc=15.5 spac=0.5  
x.mesh loc=16.0 spac=0.5  
x.mesh loc=20.5 spac=0.5  
x.mesh loc=19.0 spac=0.5  
x.mesh loc=25 spac=0.5  
y.mesh loc=-.5 spac=0.2  
y.mesh loc=-.25 spac=0.2  
y.mesh loc=0 spac=0.1  
y.mesh loc=0.75 spac=0.05  
y.mesh loc=1.0 spac=0.05  
y.mesh loc=1.15 spac=0.05  
y.mesh loc=2.20 spac=0.1
```

Figure 3.3. Specify the Mash in Silvaco Atlas for SAM InGaAs/InP APD.

Notice that for each command (x.mesh or y.mesh) there is a corresponding location (loc) and spacing (spac) command. These set boundaries for different special resolutions in the simulation.

For every change in region, material, doping, electrode etc., in the x direction, there should be a restructure of the mesh with a new location command (this is true even if the spacing remains the same during the change). The resulting mesh can be seen in Figure 3.4. The location and spacing units are in microns. The setup of the MESH is probably the most important part of the simulation when it comes to runtime efficiency, resolution of results, and convergence issues. If the mesh is too narrow then the simulation could take very long time (days) to converge. If it is too broad then the results will be either faulty due to the loss of features or insufficiently resolved. It takes quite a bit of time to get used to setting up meshes where the simulations run efficiently and the results

maintain their integrity. Once the mesh is setup, every portion of the mesh must be assigned to a REGION.

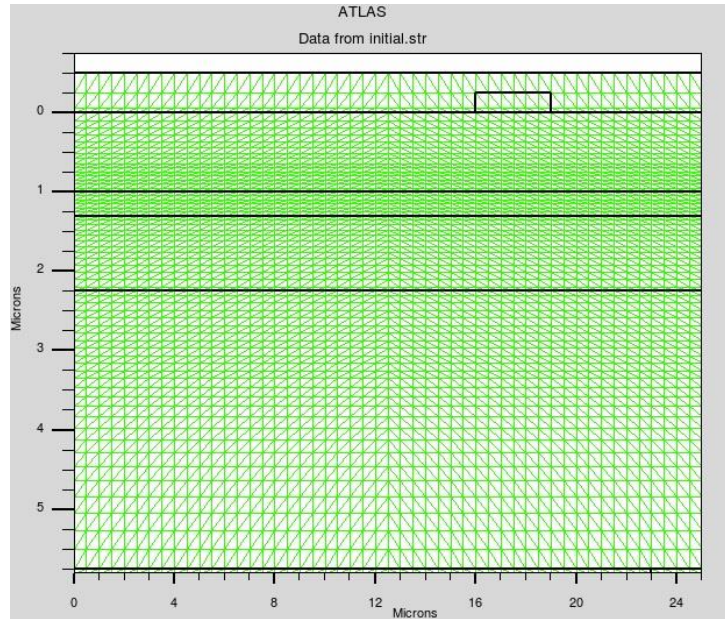


Figure 3.4. Mesh for the SAM InGaAs/InP APD. The mesh was produced in SILVACO. Proper mesh setup is necessary for accurate solutions.

3.9.2 Region Define

The regions are simply geometric assignments for different materials. The MATERIAL command is used in conjunction with the region command and can be seen by this section of code that represented in the Figure 3.5. It should also be noted that every section of the mesh must have a corresponding region and material assigned to it. There are a wide variety of materials that can be chosen as seen in the code above. The x.min, x.max, y.min and y.max commands specify the location of the regions/materials and the units stay consistent (microns) with those used when defining the mesh. Notice in the this section of code that shown in the Figure 3.5, region number 2 and 3 have been assigned composition numbers (x.comp and y.comp) based upon the Equation 3.11 [34].

```

APD.in - Deckbuild
File Edit Search Format View Commands Execution Help
[Icons]
[Navigation Icons]
###Region #####
region num=1 material=InP x.min=0 x.max=25 y.min=2.25 y.max=5.75
region num=2 material=InGaAs x.min=0 x.max=25 y.max=2.25 y.min=1.15 x.comp=.47
region num=3 material=InGaAsP x.min=0 x.max=25 y.max=1.15 x.comp=.47 y.comp=1 grad.34=.15
region num=4 material=InP x.min=0 x.max=25 y.min=0 y.max=1

```

Figure 3.5. The regions and materials that have been assigned in this Silvaco Atlas for SAM APD simulation.

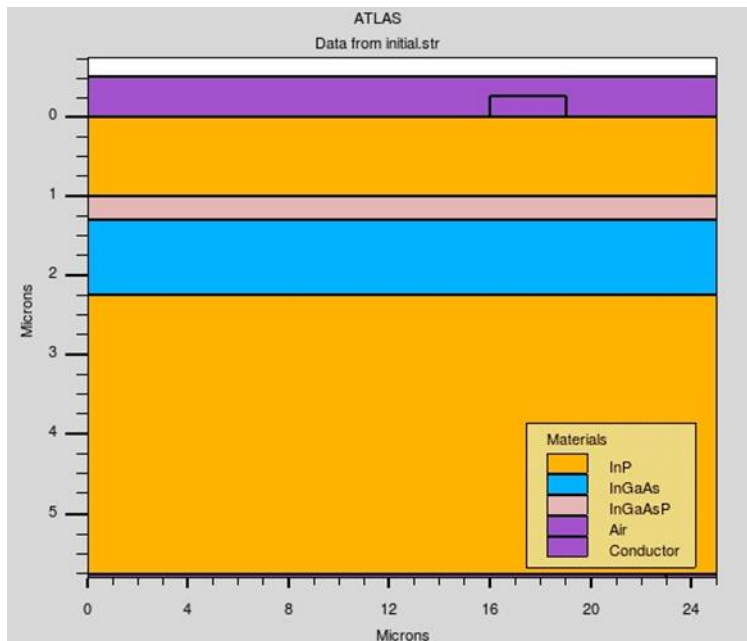


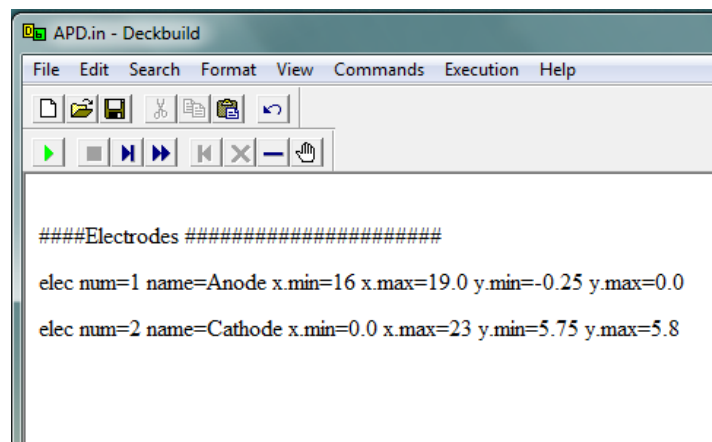
Figure 3.6. The cross section of SAM structure after assigning regions and materials in the simulation.

$$E_g = 1.35 + x(0.642 + 0.758x) + y(0.101y - 1.101) - xy(0.28x - 0.109y + 0.159) \quad (\text{Equation 3.11})$$

Where 1.35 eV is the energy gap of pure InP and the x and y composition factors alter the material in the following manner $\text{In}_{1-x}\text{Ga}_x\text{As}_y\text{P}_{1-y}$. If the x and y composition both are zero then the material is simply InP. By grading (grad.34=.15) the x composition from zero to ~1/2 and the y composition from zero to one a seamless transition is made from InP to InGaAs in the InGaAsP. This grading will smooth discontinuities in the heterojunction between the materials and eliminate anomalous barriers. The region setup per Silvaco can be seen in Figure 3.6.

3.9.3 Electrodes

Once the regions and materials are specified ELECTRODES are assigned to different locations. The electrodes geometries must be in contact with a suitable material. The electrodes are used to specify where voltages and currents can be applied to the device. It is effectively like adding a contact of some sort to the semiconductor material. The code is shown in the Figure 3.7.



```

APD.in - Deckbuild
File Edit Search Format View Commands Execution Help
#####Electrodes #####
elec num=1 name=Anode x.min=16 x.max=19.0 y.min=-0.25 y.max=0.0
elec num=2 name=Cathode x.min=0.0 x.max=23 y.min=5.75 y.max=5.8

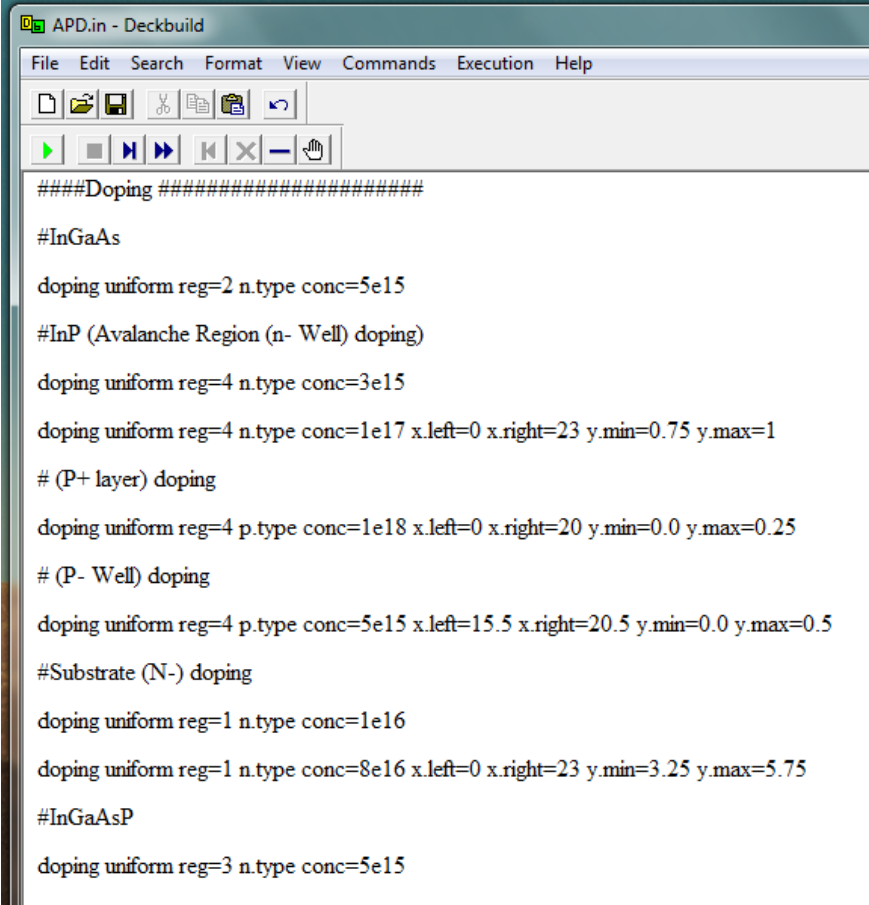
```

Figure 3.7. Assigning the electrodes to the APD structure in two different locations.

Each electrode must be named and numbered for future application of voltages and other material/contact information.

3.9.4 Doping

DOPING is the next thing to be specified. There are many different ways to specify the doping in Silvaco. The junction can be specified to be very abrupt or a gradient. The doping concentration in the well can be uniform, Gaussian or graded in nature. Figure 3.8 shows an example of how the doping was specified for the regions of the SAM APD:



```
APD.in - Deckbuild
File Edit Search Format View Commands Execution Help
#####Doping #####
#InGaAs
doping uniform reg=2 n.type conc=5e15
#InP (Avalanche Region (n- Well) doping)
doping uniform reg=4 n.type conc=3e15
doping uniform reg=4 n.type conc=1e17 x.left=0 x.right=23 y.min=0.75 y.max=1
# (P+ layer) doping
doping uniform reg=4 p.type conc=1e18 x.left=0 x.right=20 y.min=0.0 y.max=0.25
# (P- Well) doping
doping uniform reg=4 p.type conc=5e15 x.left=15.5 x.right=20.5 y.min=0.0 y.max=0.5
#Substrate (N-) doping
doping uniform reg=1 n.type conc=1e16
doping uniform reg=1 n.type conc=8e16 x.left=0 x.right=23 y.min=3.25 y.max=5.75
#InGaAsP
doping uniform reg=3 n.type conc=5e15
```

Figure 3.8. Specifying the doping profile for all regions of SAM APD in Silvaco Atlas.

Note that the pound sign (#) is for comments within the code. When an entire region is to be doped the same, there is no need for the x and y specifications. In this case all that is needed is the doping type and concentration. This is seen for regions 1, 2 and 3. Figure 3.9 shows the doping profile for the APD produced by Silvaco.

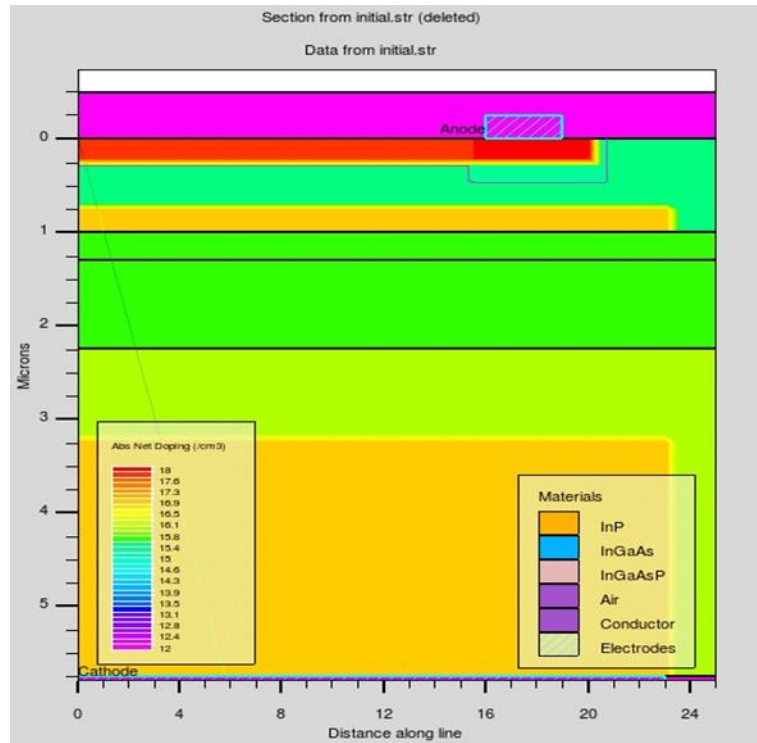


Figure 3.9. Cross section of the SAM APD doping profile as produce by Silvaco.

After the doping all that is left for the structure setup is to specify the electrode material. In this case aluminum was used and specified as shown in the Figure 3.10.

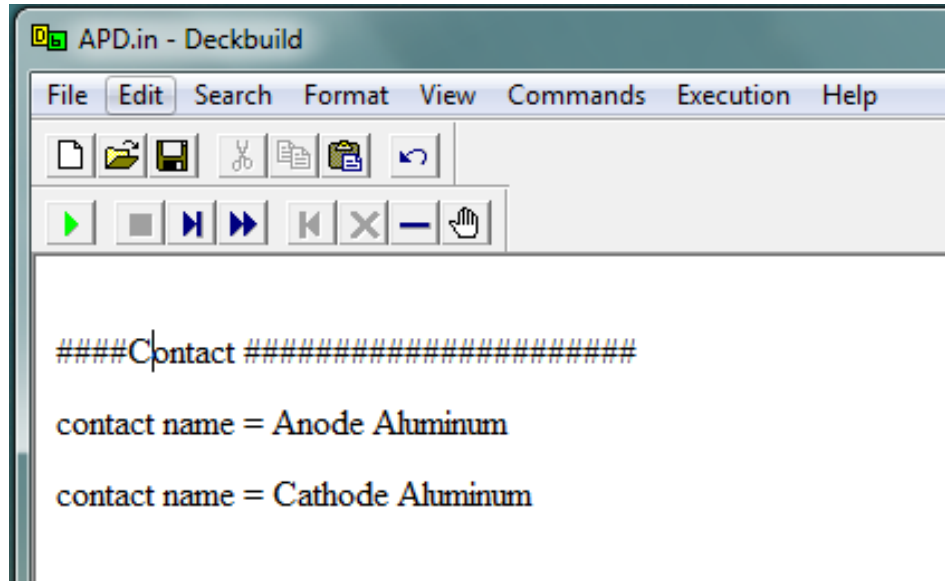


Figure 3.10. Assigning the electrodes material to the structure.

3.9.5 Model and method

The peripherals are setup the models and methods must be specified. The models used in Silvaco are based upon variations of the drift-diffusion model [34]. When specifying different models in Silvaco it is essentially telling Silvaco to focus on certain parts of the model or add additional equations to the base model equations to enhance the solution set. In this case the models specified in the simulation code are shown in section A of Figure 3.11. Table 3.2 shows the models and some brief notes about the model. In this simulation the Newton method was specified as numerical method which in the section C of Figure 3.11.

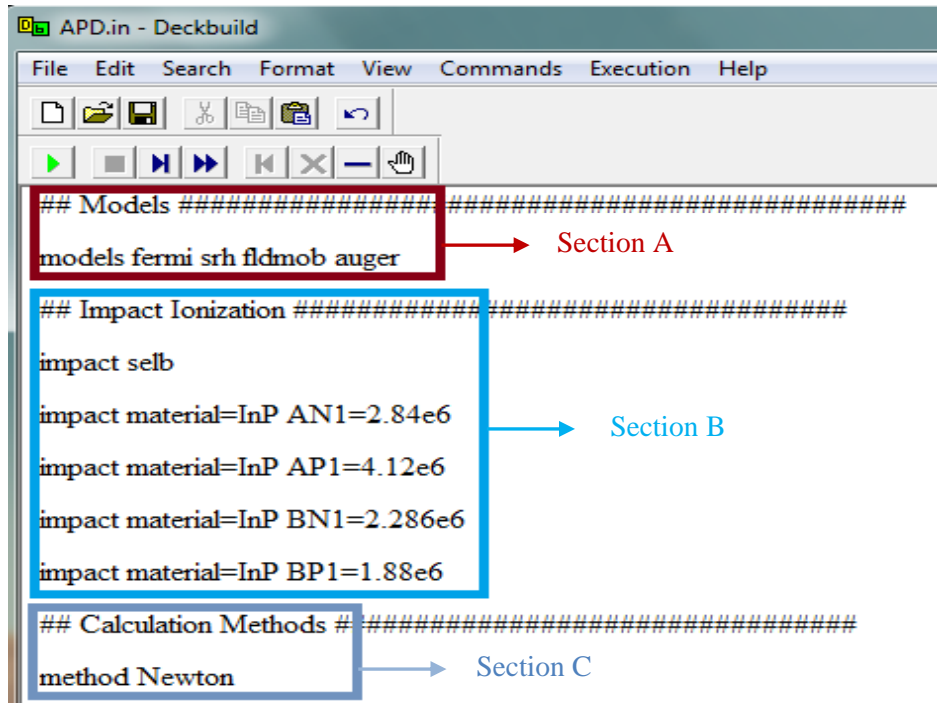


Figure 3.11. Display console of the models and calculation method.

Table 3.2: Outlines a few of the models used in Silvaco simulations.

| Model | Syntax | Notes |
|--------------------|-------------|--|
| Shockley-Read-Hall | SRH | Uses fixed minority carrier lifetimes. Should be used in most simulations. |
| Auger | AUGER | Direct transition of three carriers. Important at high current densities. |
| Selberherr's Model | IMPACT SELB | Recommended for most cases. Especially those involving impact ionization |

3.9.6 Light source

For APD simulation or any other photodiodes the light source must be specified and simulated as well. In this case the light source was specified using the BEAM command as shown in the Figure 3.12 section A. The origin of the light source is specified as well as the angle and wavelength (in microns). To make sure you have the location of the beam in the right spot and the wavelength correctly specified, Silvaco allows you to see the photogeneration rate in the semiconductor as shown in 3.13. From this point the only thing left to do is specify the intensity of the beam and apply voltage to the specified electrodes and can be done as shown in the Figure 3.12 Sections B and C respectively.

```
APD.in - Deckbuild
File Edit Search Format View Commands Execution Help
beam num=1 x.origin=25 y.origin=-0.1 angle=90.0 wavelength=1.55 rays=200 gaussian x.mean=-0.7 xsigma=5
solve init
solve b1=1e-04
solve b1=1e-03
solve b1=1e-02
solve b1=1e-01
save out=APD_P822.str
tonyplot APD_P822.str -set PhotoGenerationRate.set
log out=APD_P822.log
log csvf=APD_P822.csv APPEND
solve vanode=-1 vstep=-0.1 vfinal=-80 name=anode
log off
tonyplot APD822.log -overlay APD_P822.log -set apd_iv.set
```

Figure 3.12. Display the concentration of the incident light and applied voltage.

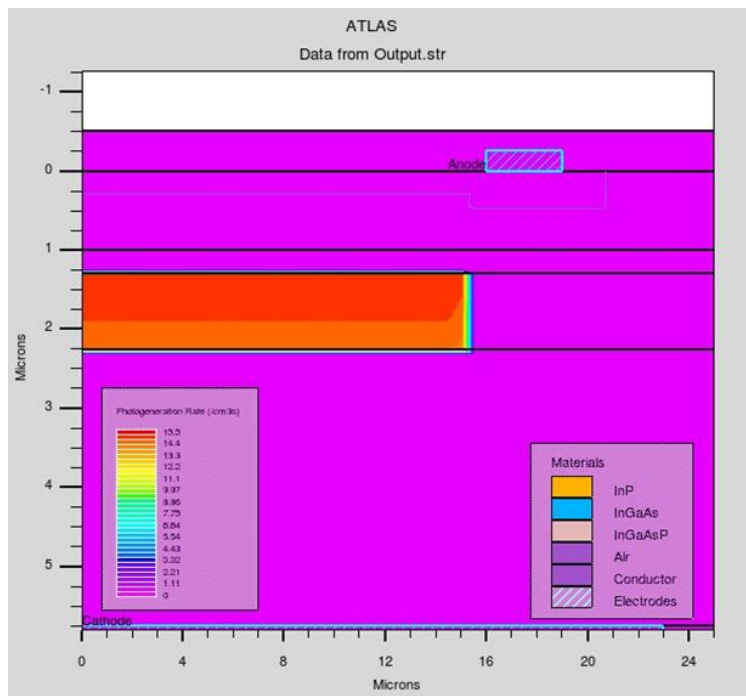


Figure 3.13. Silvaco output file showing the photogeneration rate within the device.

The units of the beam power are in Watts/cm and the units of the voltage are in Volts. The output data of the Silvaco coding can be observed in Tonyplot. Figure 3.4, 3.6, 3.9 and 3.13 give examples of a few of the cross-sectional structure diagrams viewable in Tonyplot. It is also possible to view output current versus voltage curves or the band diagrams from Silvaco for the device. For example the dark current versus voltage curve for APD can be plotted without specifying light source by using only the section C of Figure 3.12. The voltage-current curve for the simulated APD will be shown and discussed in the next chapter (section 4.1, Figure 4.1).

Silvaco has many capabilities and is very useful when trying to analyze a device and its operation before fabrication. Many of the parameters we specified above could easily be tweaked and the results viewed for comparison.

Silvaco code for simulations of the SAM, SAGM and SAGCM APD can be found in Appendix A, B and C respectively. These simulations have helped to verify designs and explore various scenarios otherwise not achievable given financial constraints.

3.10 Design of avalanche photodiode

To construct and simulated the 2-D (SAGCM) InGaAs/InP APD, general purpose 2-D device simulator, BLAZE through ALTAS was used. In Silvaco, BLAZE is applicable to a wide range of devices especially the heterojunction photodetector such as avalanche photodiode and solar cells [34]. The device cross-section of the main design of simulated APD with ALW = 2.0 μm and MLW = 0.6 μm is shown in Figure 3.14.

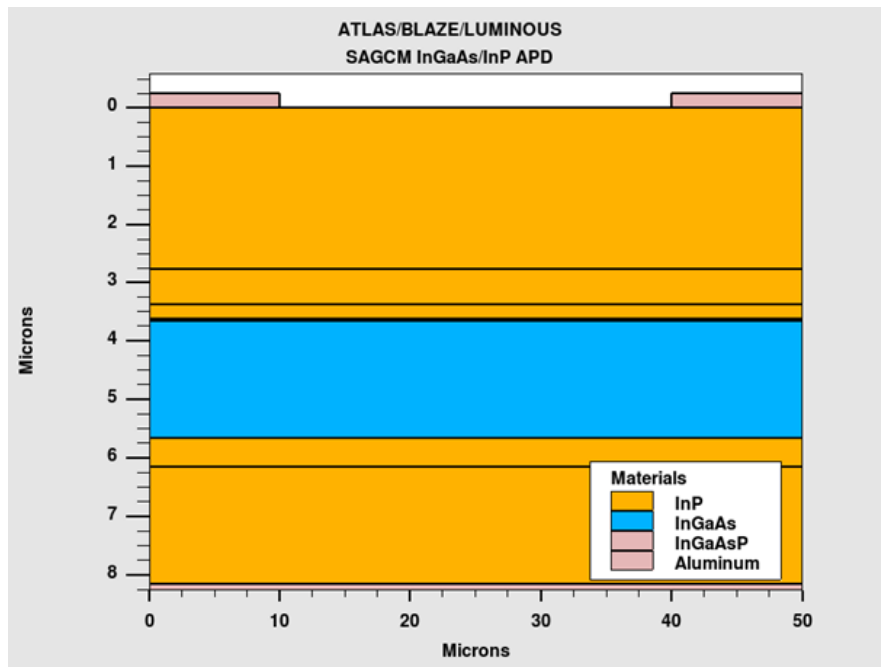


Figure 3.14. Cross section view of main design of simulation APD.

As the figure represents, an APD includes several layers and (Aluminum) electrodes (two Anodes on top and a Cathode at the bottom). These contact points were used to apply the reverse-biased voltages to the APD (Anode connect to the negative port and Cathode connect to the positive port of power supply). The fabrication of (SAGCM) InGaAs/InP APD, as shown in the Figure 3.14, start with the high doped n-type InP substrate layer and mild doped ($\sim 7 \times 10^{16}$) InP buffer layer on top of it. The next step is to grow undoped (1×10^{15}) InGaAs absorption layer followed by InP

charged layer. The purpose of the charge layer is to regulate the electric field distribution in absorption and multiplication layers. To avoid charge accumulation in heterojunction interface, several layers of InGaAsP quaternary compounds sandwiched between (InGaAs) absorption and (InP) charged layers. Finally, undoped n-type InP multiplication layer and high doped p-type InP layer are fabricated sequentially. Table 3.3 presents the structure parameters of (SAGCM) InGaAs/InP APD in the simulation. The structure parameters are similar to reference [5] except for the thickness of the multiplication layer and absorption layer, which were optimized to 0.6 μm and 2.0 μm respectively.

Table 3.3: Structure parameters for the main design of SAGCM InGaAs/InP ADP.

| Layers | Thickness (μm) | Doping (cm^{-3}) |
|--|-----------------------------|-----------------------------|
| P+-InP | 2.77 | 4×10^{17} |
| i-InP Multiplication | 0.6 | 1×10^{15} |
| n+-InP Charged | 0.25 | 1×10^{17} |
| InGaAsP Grading | 0.012 \times 3 | 1×10^{16} |
| i-In _{0.53} Ga _{0.47} As | 2.0 | 1×10^{15} |
| Absorption | | |
| InP Buffer | 0.5 | 6.6×10^{16} |
| InP Substrate | 2.0 | 3×10^{18} |

The Silvaco simulation code for the main design of simulated APD is based on the Silvaco commands that were discussed in the previous sections in this chapter and the complete code can be found in the Appendix C of this thesis.

CHAPTER 4

RESULTS AND DISCUSSION

The operation of the avalanche photodiode (APD) has been mentioned briefly in chapter 2 of this thesis. In order to show the effects of Absorption Layer Width (ALW) and Multiplication Layer Width (MLW) on the APD performance, we have varied the ALW from 1.8 μm to 2.2 μm with the step of 0.2 μm . In addition, for each ALW, the MLW has been modified from 0.2 μm to 0.8 μm with same step (0.2 μm), while the doping profile and material parameters remained unchanged. As such, several APDs with three different ALW and four MLW have been designed and simulated. The design and operation as well as the numerical results of all simulated (SAGCM) InGaAs/InP APDs will be discussed in this chapter. (The Silvaco source code that been used to simulate the performance of the SAGCM InGaAs/InP APD has been shown in Appendix C).

4.1 APD operation region

Figure 4.1 shows the comparison of the current-voltage (I - V) plot between an experimental work done in [5] and the modeled SAGCM InGaAs/InP APD, under a reversed-biased voltage for both dark and illuminated condition. It can be observed that the variation of dark current and photocurrent in APD from zero to breakdown voltage (V_b) can be divided into three primary operation regions. In region 1, the charge layer and absorption layer were not fully depleted, resulting in virtually zero collection efficiency in the case of photocurrent and the dark current is due to the thermally excited carriers in InP. In region 2, charge layer has been fully depleted, but the generated carriers still not able to transmit to the high electric field zone, therefore, there is no avalanche process, and thus the ADP operates as a unity gain photodiode. In this mode, the dark current is due to generated carrier in narrow bandgap InGaAs absorption layer, whereas, the collection efficiency of the illuminated case is near unity due to the low absorption effect. Furthermore, the depletion zone expands to the absorption layer, which at this point; the reverse-biased voltage is defines as the punch-through voltage (V_p). For region 3, the actual operation of APD begins. In this region, the V_p is high enough to deplete the (InGaAs) absorption layer entirely,

generated carriers reaching to high electric field multiplication layer. Thus, the impact ionization process will be initiated, and the device act as an APD and avalanche multiplication goes to infinity where the breakdown occurs.

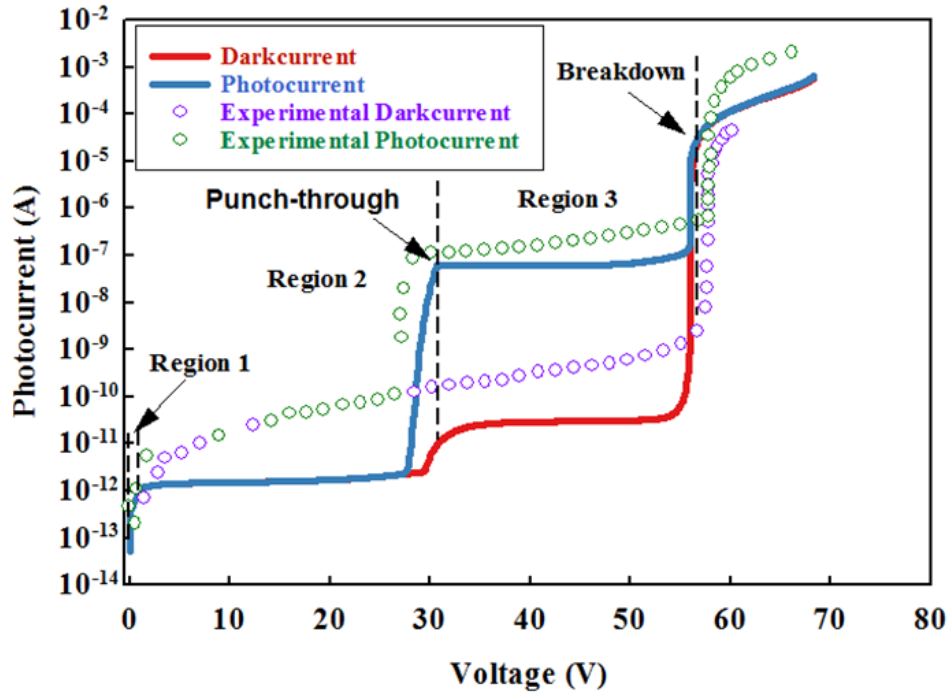


Figure 4.1. Simulated photocurrent and dark current for main APD design compare with experiment.

The V_p and the breakdown voltage, (as a voltage that the avalanche gain is infinity) is influenced by the device structure such as doping profile and layers thickness.

4.2 APD Electric field

The high electric field in an APD (Multiplication region) results in a high concentration different between highly doped p-type InP diffusion layer and un-doped n-type InP multiplication layer. Higher the concentration higher electric field which is the key parameter of avalanche process.

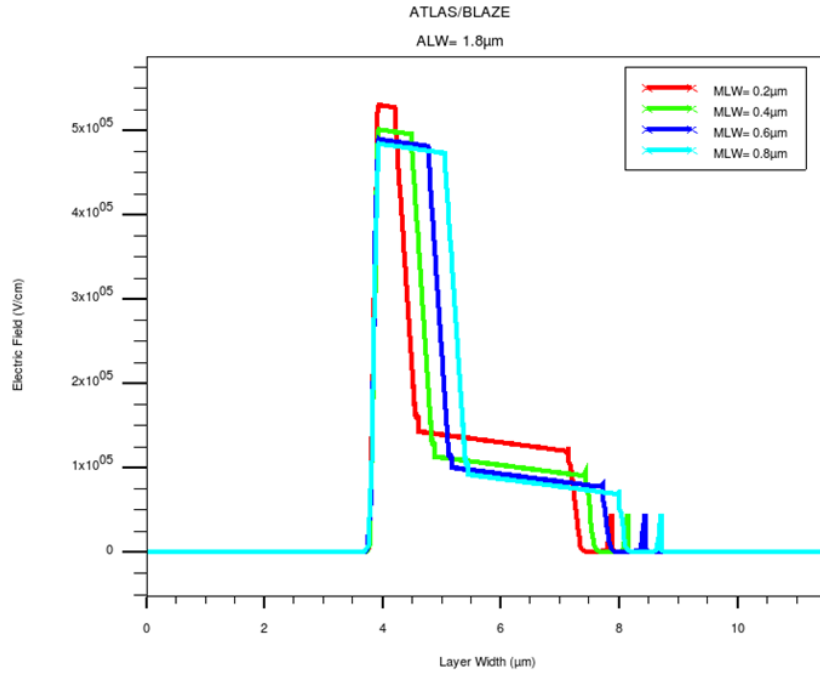


Figure 4.2. Built-in electric field for 1.8 μm ALW with vary MLW.

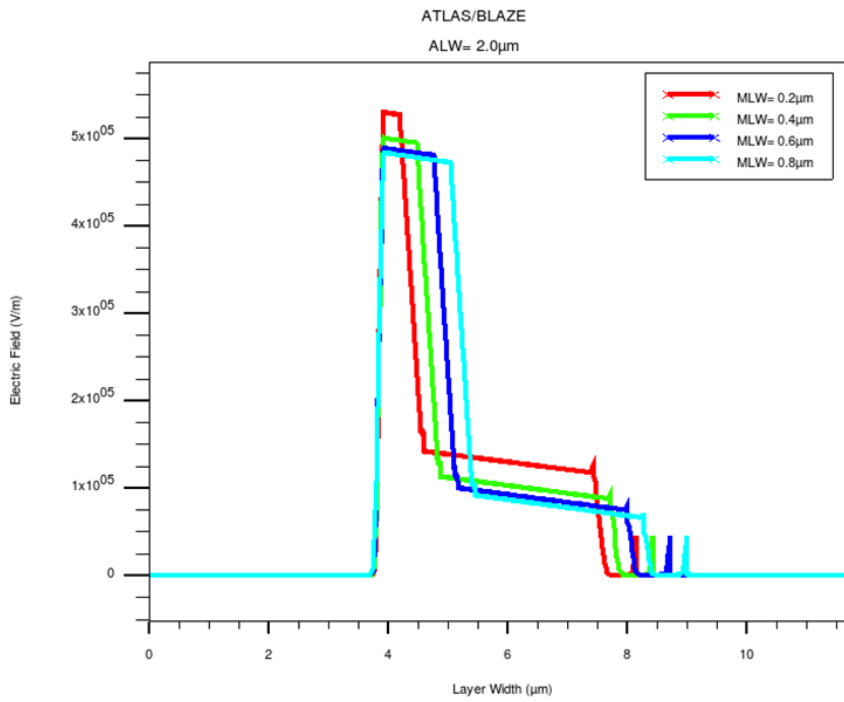


Figure 4.3. Built-in electric field for 2.0 μm ALW with vary MLW.

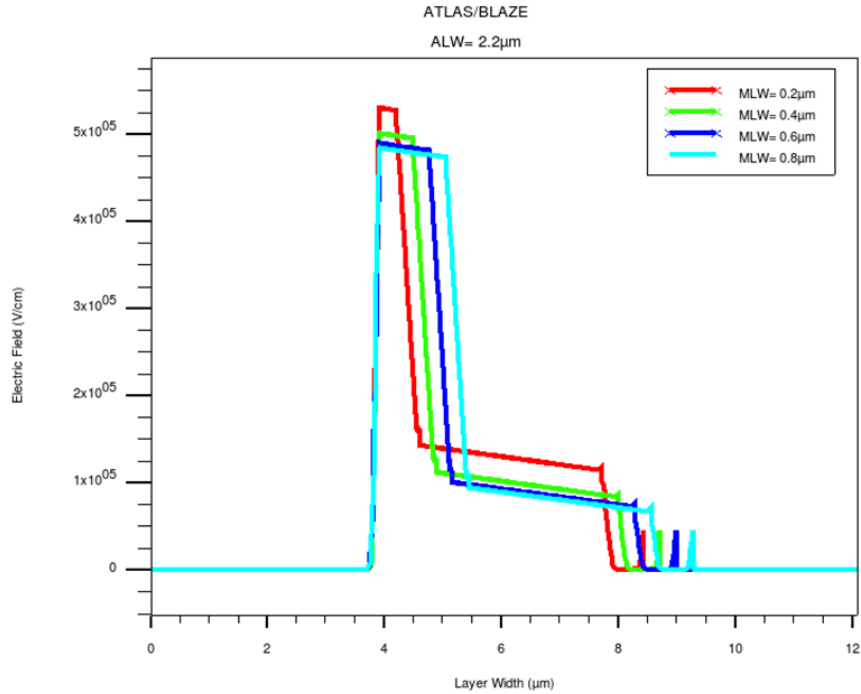


Figure 4.4. Build-in electric field for 2.2 μm ALW with vary MLW.

On the other hand, the electric field in absorption region has to be low (enough) to only separate the generated carriers (electron-hole), giving them enough energy so that they (holes) can travel to the multiplication region, and at the same time avoiding any impact ionization (or avalanching) within the absorption region. Such condition of electric field within the absorption region will be provided by punch-through voltage at which the absorption layer is fully depleted by immediate separation of generated electron-hole pairs. As such, when the carriers (holes) entered the high electric field multiplication region, they will immediately create very large number of electrons and hole pairs by impact ionization. The secondary carriers, which are generated, are further accelerated (by the mean of high electric field) and finally collected by the electrode (Anode). Meanwhile, the electrons (which is also generated in absorption region) moving towards of other electrode (Cathode). And because they are moving in the region that the electric field is not strong (or is zero), they are not able to create additional carriers and therefore, there is no avalanche process occurs there. As mentioned in the section 3.10, the regulation of electric field in the (SAGCM) InGaAs/InP APD is due to a charge layer between multiplication and absorption layers. The electric field distributions for varying MLW with three different ALW are shown in the Figure

4.2 to 4.4. As they indicate, and mentioned in chapter 2 section 2.5.2, the increment of the MLW reduces the electric field at the homojunction interface between p-type InP diffusion layer and n-type InP multiplication layer. This is because the generated carriers (holes) can travel the longer distance with a lower electric field for large MLW. Thus, they can gain enough energy at which trigger the impact ionization process. On the other hand, with smaller traveling distance of thin MLW, the electric field has to be high for carriers to reach the threshold energy to initiate impact ionization.

4.3 Photocurrent and Multiplication gain

Generally, in any charge area with sufficiently high reverse-biased voltage, the electric field will be sufficiently high to speed up the free carriers up to the point at which they will be able to acquire enough energy to generate additional free carrier pairs by collision with the atoms of the material [34]. To gain enough energy, two important conditions have to occur. First, is the high electric field as discussed in the previous section. Second, the distance between two collisions has to be short enough to allow carriers (holes) gain sufficient ionization energy. Therefore, the generation rate of free carrier pairs will be high enough to initiate the avalanche process and eventually breakdown, which in this point reverse bias voltage define as breakdown voltage. Therefore, for simulation of the avalanche process, it is necessary to calculate the generation rate of electrons and holes (G) due to impact ionization as a function of electric field. In Silvaco ATLAS this calculation is performed by [34]

$$G = \alpha |\vec{J}|_n + \beta |\vec{J}|_p \quad (\text{Equation 4.1})$$

Where, is the electrons and holes current density, α and β representing the ionization coefficient as the number of carrier pairs generated by electron-hole per unit distance traveled [34]. The impact ionization is modeled with the Selberherr model using the Equations 2.6 and 2.7 as discussed in chapter 2 section 2.4.1. In BLAZE/ATLAS, the rate of impact ionization included within basic

equation and material parameters [6][34]. All the numerical parameters for InP and InGaAs that have been used to simulate the APD performance are listed in Table 4.1 and other basic material parameters are integrated with BLAZE/ATLAS and kept as defaults. In order to simulate the performance of the designed APD under the illuminate condition the light into the APD has been set as the Gaussian form with the maximum intensity of 0.4 cd. In ATLAS the Gaussian, form the beam provides the light beam as like the beam from optical fiber [34]. The photocurrent-voltage (I_{ph} -V) curves for all the simulated structures at the temperature of 300 K are shown in Figure 4.5. ((a) ALW=1.8 μm with varying MLW, (b) ALW=2.0 μm with varying MLW and (c) ALW=2.2 μm with varying MLW from 0.2 μm to 0.8 μm .)

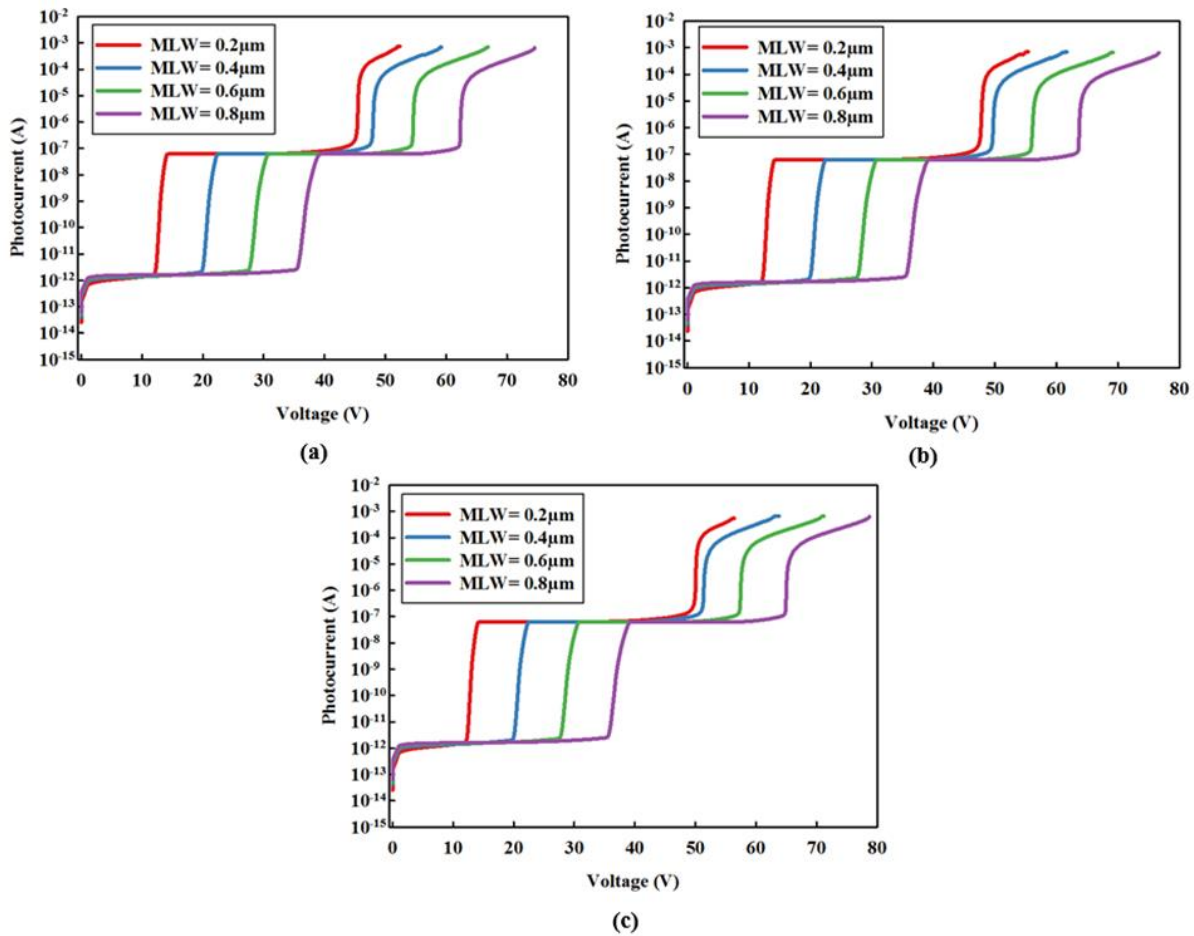


Figure 4.5. Display the I-V curves of simulated photocurrent.

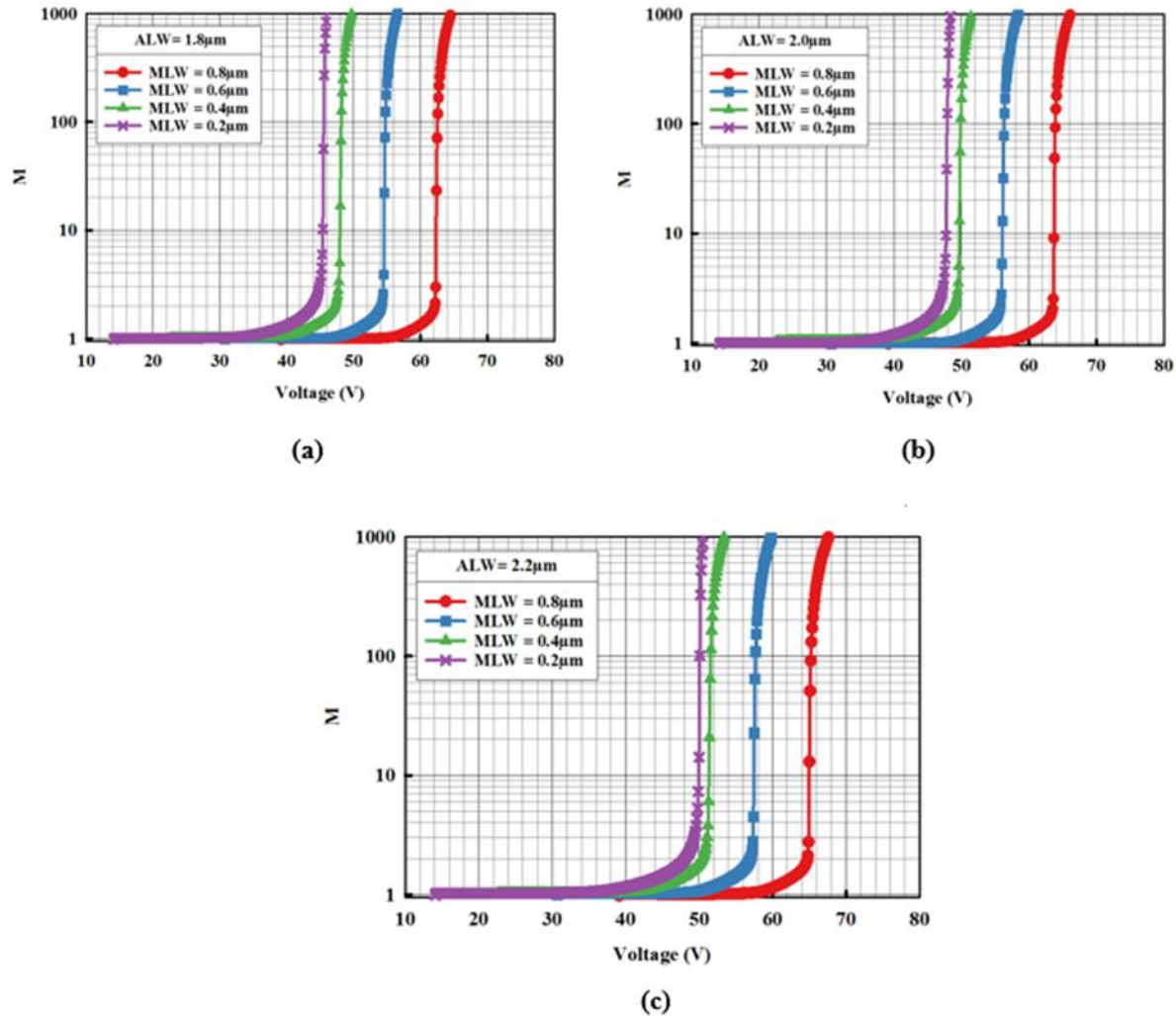


Figure 4.6. Display multiplication (M) versus Voltage (V) for all simulated structures.

Figure 4.5 also indicates that how the punch-through voltage (V_p) and breakdown voltage (V_b) change with respect to the varying MLW. As they illustrate, for the thin MLW (the APD has larger operation area than the APD with thicker MLW) or (the distance between V_b and V_p is more significant than the APD with larger MLW), and this is because the absorption layer of APD with thin MLW requires lower V_p to be fully depleted. Therefore, it can be seen from the Figure 4.6 that the APD with thin MLW has more extended operation region.

Table 4.1: Material parameters of SAGCM InGaAs/InP APDs in the simulation.

| Parameters | InP | | InGaAs | | InP | InGaAs |
|----------------------------|--|-----------|--|-----------|--|--|
| | Value | Ref | Value | Ref | Optimized Value | Optimized Value |
| Band-Gap | 1.34, 1.34, 1.34 eV | [5,6,31] | 0.78, 0.77, 0.77 eV | [5,6,31] | 1.34 eV | 0.77 eV |
| Electron Auger Coefficient | 3.7×10^{-31} , 3.7×10^{-31} , 9×10^{-31} cm ⁶ /s | [5,6,31] | 3.2×10^{-28} , 3.2×10^{-28} , 7×10^{-29} , 0 cm ⁶ /s | [5,6,31] | 9×10^{-31} cm ⁶ /s | 7×10^{-29} cm ⁶ /s |
| Hole Auger Coefficient | 8.7×10^{-30} , 8.7×10^{-30} , 9×10^{-31} cm ⁶ /s | [5,6,31] | 3.2×10^{-28} , 3.2×10^{-28} , 7×10^{-29} , 0 cm ⁶ /s | [5,6,31] | 9×10^{-31} cm ⁶ /s | 7×10^{-29} cm ⁶ /s |
| Electron SRH Lifetime | 1×10^{-9} , 1×10^{-9} , 6×10^{-12} s | [5,6,31] | 1×10^{-6} , 2.2×10^{-4} , 8×10^{-8} , 1 s | [5,6,31] | 6×10^{-12} s | 8×10^{-8} s |
| Hole SRH Lifetime | 1×10^{-9} , 1×10^{-9} , 6×10^{-12} s | [5,6,31] | 1×10^{-6} , 2.2×10^{-4} , 8×10^{-8} , 1 s | [5,6,31] | 6×10^{-12} s | 8×10^{-8} s |
| Electron impact ionization | 1×10^7 , 3.01×10^6 , 2.93×10^6 cm ⁻¹ | [31,39,6] | 4.677×10^7 , 5.15×10^7 , 2.27×10^6 cm ⁻¹ | [6,31,38] | 2.84×10^6 | 2.27×10^6 cm ⁻¹ |
| Hole impact ionization | 4.76×10^6 , 9.36×10^6 , 4.29×10^6 cm ⁻¹ | [6,31,39] | 8.382×10^7 , 9.96×10^7 , 3.95×10^6 cm ⁻¹ | [6,31,38] | 4.12×10^6 | 3.95×10^6 cm ⁻¹ |
| Electron critical field | 3.11×10^6 , 2.64×10^6 V/cm | [6,38] | 1.935×10^6 , 1.95×10^6 , 1.13×10^6 V/cm | [6,31,38] | 2.286×10^6 V/cm | 1.13×10^6 V/cm |
| Hole critical field | 2.55×10^6 , 2.78×10^6 , 2.11×10^6 V/cm | [6,31,38] | 2.236×10^6 , 2.27×10^6 , 1.45×10^6 V/cm | [6,31,38] | 1.88×10^6 V/cm | 1.45×10^6 V/cm |

In order to achieve multiplication gain (M), the ratio of photocurrent (I_{ph}) over primary current (I_{pr}) has been used (in logarithmic scale) as shown in the Equation 4.2.

$$M = \frac{I_{ph}}{I_{pr}} \quad (\text{Equation 4.2})$$

The I_{ph} for each point is directly achieved from I_{ph} - V curve that been simulated and shown in Figure 4.6. On the other hand, to have the primary current in the same point (as achieved for I_{ph}) the liner form of trendline equation from I_{ph} - V curve must be considered (to find the pattern of I_{ph} - V curve) which is in the following form

$$y = mx + c \quad (\text{Equation 4.3})$$

Where m and c are the slop and intercept of the line respectively. Now by replacing y with I_{pr} and x with each voltage points (V) in I_{ph} - V curve for all three operating regions of APD, the I_{pr} of APD will be defined as

$$I_{pr} = mV + c \quad (\text{Equation 4.4})$$

In this way, not only primary current (I_{pr}) based on all voltage points were taken into account, it can also guaranty that the collection efficiency of the APD has been considered and effect the multiplication gain curve. The curve of multiplication gain versus reverse bias voltage (M - V) with vary MLW (for three different ALW) while the doping profile and other numerical parameters kept unchanged are presented in the Figure 4.6.

Table 4.2: Punch-through voltage and break down voltage values for all simulated structures with their deference for each MLW.

| ALW (μm) | MLW (μm) | V_p | V_b | $V_b - V_p$ |
|-----------------------|-----------------------|-------|-------|-------------|
| 1.8 | 0.2 | 14.2 | 45.8 | 31.6 |
| | 0.4 | 22.6 | 48.5 | 25.9 |
| | 0.6 | 30.9 | 54.8 | 23.9 |
| | 0.8 | 39.4 | 62.2 | 22.8 |
| 2.0 | 0.2 | 14.2 | 48.0 | 33.8 |
| | 0.4 | 22.6 | 50.0 | 27.4 |
| | 0.6 | 30.9 | 56.0 | 25.1 |
| | 0.8 | 39.4 | 64.0 | 24.6 |
| 2.2 | 0.2 | 14.2 | 50.0 | 35.8 |
| | 0.4 | 22.6 | 52.0 | 29.4 |
| | 0.6 | 30.9 | 58.0 | 27.1 |
| | 0.8 | 39.4 | 65.2 | 25.8 |

As mentioned in section 4.1 the actual operation of APD is in the voltage point at which the InGaAs absorption layer just start to be depleted (which known as punch-through voltage). Therefore, the M - V carves shown in figure 4.6, are stared from unity at which corresponds to the punch-through voltage and below unity point has been ignored since the APD does not have any operation regarding multiplication gain.. From figure 4.6, different breakdown voltage values were observed for APDs with different MLW. Such curves are represented in Figure 4.7 with punch-through voltage included where V_b and V_p are plotted verses MLW for three ALW, 1.8 μm , 2.0 μm , and 2.2 μm respectively. Those curves all show non-monotonous dependence on the MLW.

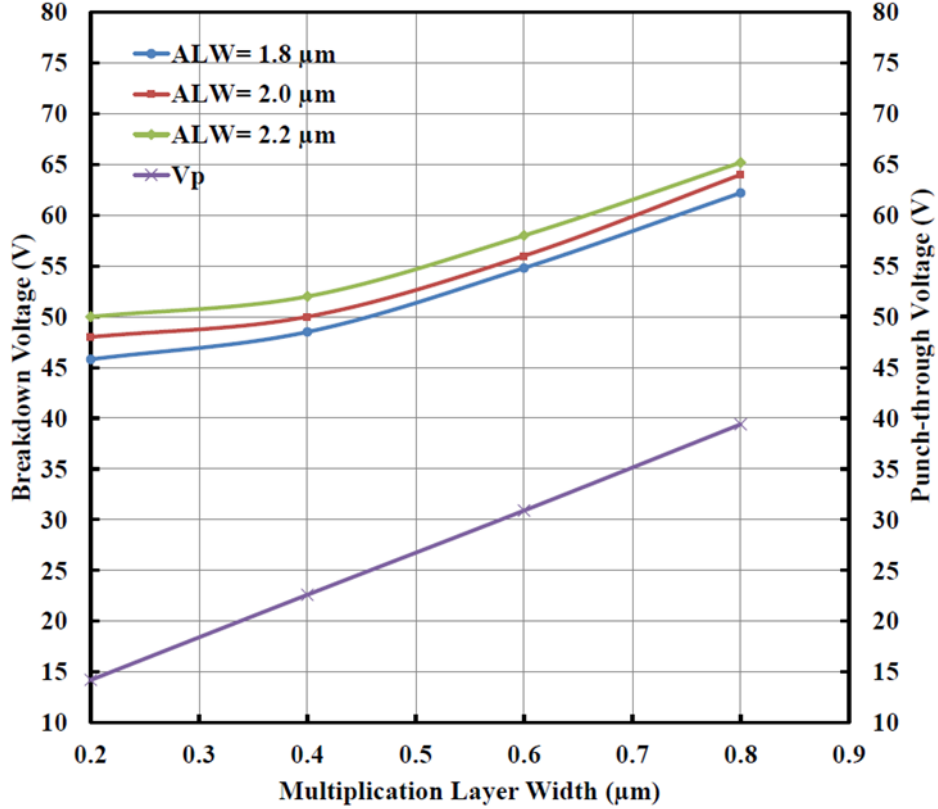


Figure 4.7. Punch-through voltage and break down voltage verses MLW for three ALW as labeled.

This feature is qualitative consistent with photocurrent simulation results in Figure 4.5 and multiplication gain in Figure 4.6. The Table 4.3 show the V_p and V_b for all simulated structures. As, it represents for $MLW \geq 0.6 \mu m$ the $V_b \geq 54.8 V$ while the deference between V_p and V_b ($V_p - V_b$) become smaller. On the other hand for $MLW \leq 0.6 \mu m$ the $V_b \leq 54.8 V$ whereas the difference between V_p and V_b is far more significant, which indicates a larger operation area. The table also present that the effects of ALW on V_b from $1.8 \mu m$ to $2.2 \mu m$ for each MLW is less than 2 V and V_p values are equal for all MLWs. However, as shown in Equation 2.27, APD with smaller ALW will decrease the carrier transmission time to the multiplication region and as results the APD response time will be decreased. Therefore, in this work the APD with ALW = $2.0 \mu m$ and MLW = $0.6 \mu m$ has been chosen as main design, so it has the sufficiently thin ALW and MLW (with $V_p - V_b = 25.1 V$). Also, it has close compatibility with experimental data as shown in Figure 4.1.

To conclude this chapter it must be mentioned that the modeling of the multiplication gain for SAGCM InGaAs/InP avalanche photodiodes designed structure has been investigated through performance simulation of three ALW with vary MLW. From the simulation results, the APD characteristics, such as the multiplication gain and the voltage breakdown, were correlated to characteristic variations of the APD. It was also found that the thickness of the InP multiplication layer width is critical for the characterization of avalanche breakdown and punch-through voltage. Moreover, it also affects the APD operation region since it can dominate the distance between punch-through voltage and breakdown voltage.

CHAPTER 5

CONCLUSION AND RECOMMENDATIONS FOR FUTURE WORK

The advancements to the avalanche photodiode have taken place in order to create a novel, quality optical detector with internal gain. The design was conceived in order to fill a hole in the long distance optical communication where the input light source could have very low intensity. More specifically, to make the separation between detection of optical signals and multiplication of the generated carriers easier and cheaper. This need arises when analyzing current optical systems. Many systems utilize photodiodes in conjunction with slow, noisy transistor based amplifiers. The introduction of a SAGCM InGaAs/InP APD makes a separation between the absorption layer and multiplication layer with several extra layers sandwich in between which can make the gain amplification performance of an APD more reliable as a semiconductor structure.

5.1 Conclusions

This dissertation outlined the study and research of the InGaAs/InP APD. This device with internal gain was designed with the intent of improving present day optical detection systems. The background behind this effort was established in Chapter 1. There, it was established that there is a need for the study and improvement of APDs. Such a device would be capable of utilizing impact ionization for gain and accepting very low-intensity light source as the input. In Chapter 2 the theory behind its APD operation was established. The impact ionization process, Electric field as well as the effects of ALW and MLW has been discussed. Chapter 3 outlined the development of device simulation software platforms. It also outlined the numerical methods used in APD simulations. The example of a SAM APD in the Silvaco platform has been illustrated. Chapters 4 discussed the alterations of the current through all three operating regions of the APD. The discussion of these alterations have been based on study, literature review, optimization and simulation of overall performance and optimized material parameters of the InGaAs/InP APD (through simulating of electric fields, photocurrent, avalanche process as a function of electric field and calculation of multiplication gain due to collection efficiency effect of the APD).

To sum up, in this dissertation, extensive investigation and study were done to carry out a list of III-V semiconductor material physical parameters which are suitable for (SAM, SACM, and SAGCM) InGaAs/InP APD design using Silvaco obtained through comparison between the simulation results and the experimental results. Modeling of the avalanche gain for SAGCM InGaAs/InP avalanche photodiodes designed structure has been carried out through the simulation of three ALW with varying MLW. From the simulation results, the APD characteristics, such as the dark current, photocurrent and the voltage breakdown, were outlined. The relationship between the ALW and MLW regarding avalanche gain was formulated. It was also found that the thickness of the InP multiplication layer is critical for characterization of avalanche breakdown and punch-through voltage. Furthermore, it affects the APD operation region since it can dominate the distance between punch-through voltage and breakdown voltage. Finally, the future work remains for the development of what still has potential to be an important device in modern day optical detection systems.

5.2 Future Work

From the information outlined in the previous chapters, the most glaring future work is the realization and characterization of the optimal APD structure. The realization of this device was just out of reach. The theory behind its improved functionality has been outlined. The simulation and modeling to support this theory has also been explored. With sufficient time and resources, the optimal design of the APD can be realized with confidence. Further characterization of the frequency response are also included in future efforts which can be obtained from the impulse response by fast Fourier transformation. The excess noise characteristics of the APD have never been well established since it is corresponding to the higher electric field for ionization process for thinner multiplication layer. The APD is very special in structure and purpose, which makes these efforts necessary in future analysis.

REFERENCES

- [1] Bhattacharya, P. (2009). Semiconductor optoelectronic devices. New Delhi: Prentice Hall India.
- [2] Fukuda, M. (1999). Optical semiconductor devices. New York [u.a.]: Wiley.
- [3] Saleh, B. and Teich, M. (2007). Fundamentals of photonics. Hoboken,NJ: Wiley.
- [4] Senior, J. and Jamro, M. (2009). Optical fiber communications. Harlow, England: Financial Times/Prentice Hall.
- [5] Xu, J., Chen, X., Wang, W. and Lu, W. (2016). Extracting dark current components and characteristics parameters for InGaAs/InP avalanche photodiodes. *Infrared Physics & Technology*, 76, pp.468-473.
- [6] Parks, J., Smith, A., Brennan, K. and Tarof, L. (1996). Theoretical study of device sensitivity and gain saturation of separate absorption, grading, charge, and multiplication InP/InGaAs avalanche photodiodes. *IEEE Transactions on Electron Devices*, 43(12), pp.2113-2121.
- [7] Zeng, Q., Wang, W., Wen, J., Xu, P., Hu, W., Li, Q., Li, N. and Lu, W. (2014). Dependence of dark current on carrier lifetime for InGaAs/InP avalanche photodiodes. *Optical and Quantum Electronics*, 47(7), pp.1671-1677
- [8] Susa, N., Nakagome, H., Ando, H. and Kanbe, H. (1981). Characteristics in InGaAs/InP avalanche photodiodes with separated absorption and multiplication regions. *IEEE Journal of Quantum Electronics*, 17(2), pp.243-250.
- [9] Zhao, Y., Zhang, D., Qin, L., Tang, Q., Wu, R., Liu, J., Zhang, Y., Zhang, H., Yuan, X. and Liu, W. (2011). InGaAs–InP avalanche photodiodes with dark current limited by generation-recombination. *Optics Express*, 19(9), p.8546.

- [10] M. Woods, W. Johnson, and M. Lampert, "Use of a Schottky barrier to measure impact ionization coefficients in semiconductors," *Solid-State Electronics*, vol. 16, no. 3, pp. 381–394, 1973
- [11] Ma, J., Bai, B., Wang, L., Tong, C., Jin, G., Zhang, J. and Pan, J. (2016). Design considerations of high-performance InGaAs/InP single-photon avalanche diodes for quantum key distribution. *Applied Optics*, 55(27), p.7497.
- [12] Acerbi, F., Tosi, A. and Zappa, F. (2013). Growths and diffusions for InGaAs/InP single-photon avalanche diodes. *Sensors and Actuators A: Physical*, 201, pp.207-213.
- [13] C. Ma, Characterization and modelling of SAGCM InP/InGaAs avalanche photodiodes for multigigabit optical fiber communications. Ottawa: National Library of Canada, 1996.
- [14] H. T. J. Meier, Design, characterization and simulation of avalanche photodiodes. Zürich: ETH, 2011.
- [15] Saleh, M., Hayat, M., Sotirelis, P., Holmes, A., Campbell, J., Saleh, B. and Teich, M. (2001). Impact-ionization and noise characteristics of thin III-V avalanche photodiodes. *IEEE Transactions on Electron Devices*, 48(12), pp.2722-2731.
- [16] Welch, D., Kish, F., Melle, S., Nagarajan, R., Kato, M., Joyner, C., Pleumeekers, J., Schneider, R., Back, J., M. and Mehuys, D. (2007). Large-Scale InP Photonic Integrated Circuits: Enabling Efficient Scaling of Optical Transport Networks. *IEEE Journal of Selected Topics in Quantum Electronics*, 13(1), pp.22-31.
- [17] P. S. A. Roslan, P. J. Ker, I. Ahmad, J. Pasupuleti, and P. Z. Fam, "Modeling and simulation of InAs photodiode on electric field profile and dark current characteristics," 2016 IEEE International Conference on Semiconductor Electronics (ICSE), 2016.
- [18] O'Reilly, J. and Fyath, R. (1988). Analysis of the influence of dark current on the performance of optical receivers employing superlattice APDs. *IEE Proceedings J Optoelectronics*, 135(2), p.109.

- [19] Fyath, R. and O'Reilly, J. (1989). Performance degradation of APD-optical receivers due to dark current generated within the multiplication region. *Journal of Lightwave Technology*, 7(1), pp.62-67.
- [20] Ma, C., Deen, M. and Tarof, L. (1995). Multiplication in separate absorption, grading, charge, and multiplication InP-InGaAs avalanche photodiodes. *IEEE Journal of Quantum Electronics*, 31(11), pp.2078-2089.
- [21] An, S. and Deen, M. (2000). Low-frequency noise in single growth planar separate absorption, grading, charge, and multiplication avalanche photodiodes. *IEEE Transactions on Electron Devices*, 47(3), pp.537-543.
- [22] Chen, Y., Wun, J., Wu, S., Chao, R., Huang, J., Jan, Y., Chen, H., Ni, C., Chang, H., Chou, E. and Shi, J. (2018). Top-Illuminated In_{0.52}Al_{0.48}As-Based Avalanche Photodiode With Dual Charge Layers for High-Speed and Low Dark Current Performances. *IEEE Journal of Selected Topics in Quantum Electronics*, 24(2), pp.1-8.
- [23] Tien-Pei Lee, Burrus, C. and Dentai, A. (1981). InGaAs/InP p-i-n photodiodes for lightwave communications at the 0.95-1.65 μm wavelength. *IEEE Journal of Quantum Electronics*, 17(2), pp.232-238.
- [24] P. Yuan, K. Anselm, C. Hu, H. Nie, C. Lenox, A. Holmes, B. Streetman, J. Campbell, and R. McIntyre, "A new look at impact ionization-Part II: Gain and noise in short avalanche photodiodes," *IEEE Transactions on Electron Devices*, vol. 46, no. 8, pp. 1632–1639, 1999.
- [25] P. Yuan, C. Hansing, K. Anselm, C. Lenox, H. Nie, A. Holmes, B. Streetman, and J. Campbell, "Impact ionization characteristics of III-V semiconductors for a wide range of multiplication region thicknesses," *IEEE Journal of Quantum Electronics*, vol. 36, no. 2, pp. 198–204, 2000.
- [26] G. M. Williams, M. Compton, D. A. Ramirez, M. M. Hayat, and A. S. Huntington, "Multi-Gain-Stage InGaAs Avalanche Photodiode With Enhanced Gain and Reduced Excess Noise," *IEEE Journal of the Electron Devices Society*, vol. 1, no. 2, pp. 54–65, 2013.

- [27] R. Fyath and J. Oreilly, "Performance degradation of APD-optical receivers due to dark current generated within the multiplication region," *Journal of Lightwave Technology*, vol. 7, no. 1, pp. 62–67, 1989.
- [28] J. Chen, Z. Zhang, M. Zhu, J. Xu, and X. Li, "Optimization of InGaAs/InAlAs Avalanche Photodiodes," *Nanoscale Research Letters*, vol. 12, no. 1, 2017.
- [29] J. Tu, Y. Zhao, K. Wen, Q. Li, and Y. Li, "The Determination of Unity Gain for InGaAs/InP Avalanche Photodiodes With Excess Noise Measurements," *IEEE Photonics Technology Letters*, vol. 29, no. 8, pp. 671–674, 2017.
- [30] M. H. Mun, S. W. Jung, H. Kang, D. Kim, H. J. Kim, S. H. Lee, and H. Park, "Design and Simulation Result of N Substrate Reverse Type Avalanche Photodiode (APD)," *IEEE Transactions on Nuclear Science*, vol. 56, no. 3, pp. 1046–1050, 2009.
- [31] J. K. Park and I. Yun, "Modeling of avalanche gain for high-speed InP/InGaAs avalanche photodiodes," 2008 IEEE International Conference on Electron Devices and Solid-State Circuits, 2008.
- [32] G.-F. D. Betta, L. Pancheri, M. Boscardin, G. Paternoster, C. Piemonte, N. Cartiglia, F. Cenna, and M. Bruzzi, "Design and TCAD simulation of double-sided pixelated low gain avalanche detectors," *Nuclear Instruments and Methods in Physics Research Section A: Accelerators, Spectrometers, Detectors and Associated Equipment*, vol. 796, pp. 154–157, 2015.
- [33] Silvaco Standard Simulation, Two-Dimensional Device Simulation of InGaAs/InP Avalanche Photodiode, 2014
- [34] V. Palankovski, Analysis and simulation of heterostructure devices. Place of publication not identified: Springer Verlag GmbH, 2012.
- [35] ATLAS User's Manual—Device Simulation Software Silvaco, 2016
- [36] Marshall, A., David, J. and Tan, C. Impact Ionization in InAs Electron Avalanche Photodiodes. *IEEE Transactions on Electron Devices*, 57(10), pp.2631-2638. 2010

- [37] Saleh, M., Hayat, M., Sotirelis, P., Holmes, A., Campbell, J., Saleh, B., & Teich, M. (2001). Impact-ionization and noise characteristics of thin III-V avalanche photodiodes. *IEEE Transactions on Electron Devices*, 48(12), 2722-2731. doi:10.1109/16.974696
- [38] S. L. Chuang, *Physics of photonic devices*. Hoboken, NJ: John Wiley & Sons, 2009.
- [39] Saleh, M., Hayat, M., Sotirelis, P., Holmes, A., Campbell, J., Saleh, B., & Teich, M. (2001). Impact-ionization and noise characteristics of thin III-V avalanche photodiodes. *IEEE Transactions on Electron Devices*, 48(12), 2722-2731. doi:10.1109/16.974696
- [40] Jackson, J. C., Hurley, P. K., Lane, B., Mathewson, A., & Morrison, A. P. (2002). Comparing leakage currents and dark count rates in Geiger-mode avalanche photodiodes. *Applied Physics Letters*, 80(22), 4100-4102. doi:10.1063/1.1483119
- [41] R. Yeats and S. H. Chiao, "Leakage current in InGaAsP avalanche photodiodes," *Applied Physics Letters*, vol. 36, no. 2, pp. 167–170, 1980.

APPENDIX A

go atlas

mesh space.mult=1.0

#-----

#SET UP MESH

#-----

x.mesh loc=0.0 spac=0.5

x.mesh loc=15.5 spac=0.5

x.mesh loc=16.0 spac=0.5

x.mesh loc=20.5 spac=0.5

x.mesh loc=19.0 spac=0.5

x.mesh loc=23 spac=0.5

y.mesh loc=-0.5 spac=0.2

y.mesh loc=-0.25 spac=0.2

y.mesh loc=0 spac=0.1

y.mesh loc=0.75 spac=0.05

y.mesh loc=1.0 spac=0.05

y.mesh loc=1.15 spac=0.05

y.mesh loc=2.20 spac=0.1

y.mesh loc=2.25 spac=0.1

y.mesh loc=2.3 spac=0.1

y.mesh loc=3.25 spac=0.1

y.mesh loc=5.75 spac=0.25

y.mesh loc=5.8 spac=0.25

```

#-----
# Set up Regions
#-----
#going from Substrate up
region num=1 material=InP x.min=0 x.max=23 y.min=2.25 y.max=5.75
region num=2 material=InGaAs x.min=0 x.max=23 y.max=2.25 y.min=1.15 x.comp=.47
region num=3 material=InGaAsP x.min=0 x.max=23 y.max=1.15 x.comp=.47 grad.34=.15
region num=4 material=InP x.min=0 x.max=23 y.min=0 y.max=1
region num=5 material=Air x.min=0 x.max=23 y.min=-.5 y.max=0
region num=6 material=Air x.min=0 x.max=23 y.min=5.75 y.max=5.8

#-----
# SET UP ELECTRODES
#-----
elec num=1 name=Anode x.min=16 x.max=19.0 y.min=-0.25 y.max=0.0
elec num=2 name=Cathode x.min=0.0 x.max=23 y.min=5.75 y.max=5.8
#-----
# SET UP DOPING
#-----
#InGaAs
doping uniform reg=2 n.type conc=5e15
#InP
#Avalanche Region(n- Well) doping
doping uniform reg=4 n.type conc=3e15
doping uniform reg=4 n.type conc=1e17 x.left=0 x.right=23 y.min=0.75 y.max=1
#(P+ layer) doping
doping uniform reg=4 p.type conc=1e18 x.left=0 x.right=20 y.min=0.0 y.max=0.25
#(P- Well) doping
doping uniform reg=4 p.type conc=5e15 x.left=15.5 x.right=20.5 y.min=0.0 y.max=0.5

```

```

#Substrate (n-) doping
doping uniform reg=1 n.type conc=1e16
doping uniform reg=1 n.type conc=8e16 x.left=0 x.right=23 y.min=3.25 y.max=5.75
#InGaAsP Graded doping
doping uniform reg=3 n.type conc=5e15

#Check structure
#-----
# SET UP MATERIAL & MODEL
#-----
material material=InP
material material=InGaAs

models srh bbt.kl auger consrh impact selb
#material material=InGaAs sopra=Ingaas.nk
#material material=Inp sopra=Inp.nk

#-----
# SET UP CONTACTS
#-----
contact name = Anode Aluminum
contact name = Cathode Aluminum
#-----
#Light Source
#-----
beam num=1 x.origin=5 y.origin=-1.0 angle=90.0 wavelength=1.55 max.window=5
#-----
# SOLVE
#-----

```

```
impact selb
output con.band val.band band.param photogen
solve init

method Newton
log outf=Output.log

save outfile=initial.str
tonyplot initial.str

solve b1=1e-7
solve b1=1e-6
solve b1=1e-5
solve b1=0.001
solve b1=0.01
solve b1=0.05
solve b1=0.075
solve b1=0.1
solve b1=0.3
solve b1=0.5
solve b1=0.75
solve b1=1.0

solve vAnode=0
solve vAnode=-.001
solve vAnode=-.01
solve vAnode=-.1
solve vAnode=-1 vstep=-1 name=Anode vfinal=-40
```

```
save outfile=Output.str
```

```
tonyplot Output.str
```

```
tonyplot Output.log
```

```
Quit
```

APPENDIX B

Go Atlas

```
mesh space.mult=1.0
```

```
#-----
```

```
#SET UP MESH
```

```
#-----
```

```
x.mesh loc=0.0 spac=0.5
```

```
x.mesh loc=15.5 spac=0.5
```

```
x.mesh loc=16.0 spac=0.5
```

```
x.mesh loc=19.0 spac=0.5
```

```
x.mesh loc=20.5 spac=0.5
```

```
x.mesh loc=23 spac=0.5
```

```
y.mesh loc=-0.5 spac=0.2
```

```
y.mesh loc=-0.25 spac=0.2
```

```
y.mesh loc=0 spac=0.1
```

```
y.mesh loc=0.25 spac=0.05
```

```
y.mesh loc=0.5 spac=0.05
```

```
y.mesh loc=0.75 spac=0.05
```

```
y.mesh loc=1.0 spac=0.05
```

```
y.mesh loc=1.15 spac=0.05
```

```
#y.mesh loc=1.18 spac=0.05
```

```
y.mesh loc=2.20 spac=0.1
```

```
y.mesh loc=2.25 spac=0.1
```

```
y.mesh loc=2.3 spac=0.1
```

```
y.mesh loc=3.25 spac=0.1
```

y.mesh loc=5.75 spac=0.25

y.mesh loc=5.8 spac=0.25

#-----

Set up Regions

#-----

#going from Substrate up

region num=1 material=Air x.min=0 x.max=23 y.min=-0.5 y.max=0.0

region num=2 material=InP x.min=0 x.max=23 y.min=0.0 y.max=1.00

#region num=3 material=InP x.min=0 x.max=23 y.min=0.75 y.max=1.00

region num=4 material=InGaAsP x.min=0 x.max=23 y.min=1.00 y.max=1.15 x.comp=0.47 y.comp=1
grad.34=0.15

region num=5 material=InGaAs x.min=0 x.max=23 y.min=1.15 y.max=2.25 x.comp=0.47

#region num=6 material=InP x.min=0 x.max=23 y.min=2.25 y.max=5.75

#region num=7 material=Air x.min=0 x.max=23 y.min=5.75 y.max=5.8

#####

region num=6 material=InP x.min=0 x.max=23 y.min=2.25 y.max=3.5

region num=7 material=InP x.min=0 x.max=23 y.min=3.25 y.max=5.75

region num=8 material=Air x.min=0 x.max=23 y.min=5.75 y.max=5.8

#####

#-----

SET UP ELECTRODES

#-----

elec num=1 name=Anode x.min=16 x.max=19.0 y.min=-0.25 y.max=0.0

elec num=2 name=Cathode x.min=0.0 x.max=23 y.min=5.75 y.max=5.8

#-----

SET UP DOPING

#-----

#InGaAs

```

doping uniform reg=5 n.type conc=5e14
#-----
#InP (Avalanche Region(n- Well) doping)
doping uniform reg=2 n.type conc=3e14
doping uniform reg=2 n.type conc=1e17 x.left=0 x.right=23 y.min=0.75 y.max=1
#-----
#(P+ layer) doping
doping uniform reg=2 p.type conc=1e18 x.left=0 x.right=20 y.min=0.0 y.max=0.25
#-----
#(P- Well) doping
doping uniform reg=2 p.type conc=5e14 x.left=15.5 x.right=20.5 y.min=0.0 y.max=0.5
#-----
#Substrate (n-) doping
#doping uniform reg=6 n.type conc=1e16
#doping uniform reg=6 n.type conc=8e16 x.left=0 x.right=23 y.min=3.25 y.max=5.75
#####
doping uniform reg=6 n.type conc=1e16
doping uniform reg=7 n.type conc=8e16
#####
#-----
#InGaAsP Graded doping
doping uniform reg=4 n.type conc=5e15
#-----
#Check structure
#-----
# SET UP MATERIAL & MODEL
#-----

```

Material InP

From Ref[7]

material material=InP EG300=1.34 permitti=12.61 affinity=4.51 AUGN=9.0e-31 AUGP=9.0e-31
taun0=6.e-12 taup0=9.0e-12 vsatn=2.6e7 vsatp=2.6e7 MUN=4730 MUP=151 alphaa=0 copt=1.2e-10

From Ref[6]

#material material=InP EG300=1.34 permitti=12.61 affinity=4.51 AUGN=3.7e-31 AUGP=8.7e-30
taun0=1.0e-9 taup0=1.0e-9 vsatn=2.6e7 vsatp=2.6e7 MUN=4730 MUP=151 alphaa=0

#

Material InGaAs

From Ref[7]

material material=InGaAs EG300=0.77 permitti=13.85 affinity=4.7 AUGN=7.0e-29 AUGP=7.0e-29
taun0=8.0e-8 taup0=8.0e-8 vsatn=7e6 vsatp=4.9e6 MUN=12000 MUP=450 alphaa=8000 copt=9.6e-11

From Ref[6]

#material material=InGaAs EG300=0.77 permitti=13.85 affinity=4.7 AUGN=3.2e-28 AUGP=3.2e-28
taun0=2.2e-4 taup0=2.2e-4 vsatn=7e6 vsatp=4.9e6 MUN=12000 MUP=450 alphaa=8000

#

Optical Properties of Materials

material material=InGaAs sopra=Ingaas.nk

material material=Inp sopra=Inp.nk

#

contact name = Anode Aluminum

contact name = Cathode Aluminum

#

model material=InP srh optr fldmob impact selb fermidirac print conmob auger bgn bbt.kl analytic all

model material=InGaAs srh optr fldmob impact selb fermidirac print conmob auger bgn bbt.kl analytic all

bipolar consrh

impact selb

```
impact material=InP AN1=1.0e7 AP1=9.36e6 BN1=3.45e6 BP1=2.78e6
impact material=InGaAs AN1=5.15e7 AP1=9.69e7 BN1=1.95e6 BP1=2.27e6
```

```
output con.band val.band band.param photogen
```

```
method Newton
```

```
# Dark #####
```

```
solve init
```

```
log outf=OutputNew.log
```

```
solve vAnode=0
```

```
solve vAnode=-0.001
```

```
solve vAnode=-0.01
```

```
solve vAnode=-0.1
```

```
solve vAnode=-1 vstep=-1 name=Anode vfinal=-150
```

```
save outfile=initialNew.str
```

```
log off
```

```
tonyplot initialNew.str -set ElectricField.set
```

```
tonyplot OutputNew.log
```

```
#-----
```

```
#Light Source
```

```
#-----
```

```
beam num=1 x.origin=5 y.origin=-1.0 angle=90.0 wavelength=1.55 max.window=15 rays=101 gaussian
x.mean=-0.7 xsigma=5
```

```
#-----
```

```
#-----
```

```
# SOLVE
```

```
#-----
```

solve init

log outf=Output_2.log

solve b1=1e-7

solve b1=1e-6

solve b1=1e-5

solve b1=0.001

solve b1=0.01

solve b1=0.05

solve b1=0.075

solve b1=0.1

solve b1=0.3

solve b1=0.5

solve b1=0.75

solve b1=1.0

solve vAnode=0

solve vAnode=-0.001

solve vAnode=-0.01

solve vAnode=-0.1

solve vAnode=-1 vstep=-1 name=Anode vfinal=-150

tonyplot Output.str -set PhotoGenerationRate.set

tonyplot Output.str -set ElectricField.set

tonyplot Output_2.log

Quit

APPENDIX C

#####

```
# Project: InGaAs/InP Avalanche Photodiode #
# Performed By: MAHDI ALL KHAMIS #
# Supervisor: Dr Ker Pin Jern #
# Date: November 2017 #
```

#####

go atlas

Mesh Define

mesh auto

x.m loc=0.0 s=10

x.m loc=50.0 s=10

Structure Define

region material=InP bot thick=2.77 accept=4e17 ny=20

region material=InP bot thick=0.6 donors=1e15 ny=20

region material=InP bot thick=0.25 donors=1e17 ny=20

region material=InGaAsP bot thick=0.012 donors=1e16 ny=20

region material=InGaAsP bot thick=0.012 donors=1e16 ny=20

region material=InGaAsP bot thick=0.012 donors=1e16 ny=20

region material=InGaAs bot thick=2.0 donors=1e15 ny=20 x.comp=0.47

region material=InP bot thick=0.5 donors=6.6e16 ny=20

region material=InP bot thick=2.0 donors=3e18 ny=20

Electrods Define

electrode name=anode x.min=0 x.max=10 top
electrode name=anode x.min=40 x.max=50 top
electrode name=cathode bottom

Materials Parameters

material material=InP
material material=InP EG300=1.34
material material=InP taup0=6.0e-12 taun0=6.0e-12
material material=InP affinity=4.51
material material=InP permitti=12.61
material material=InP AUGN=9e-31
material material=InP AUGP=9e-31
material material=InP MUN=4730
material material=InP MUP=151
material material=InP copt=1.2e-10

material material=InGaAs
material material=InGaAs EG300=0.78
material material=InGaAs taup0=8.0e-8 taun0=8.0e-8
material material=InGaAs affinity=4.7
material material=InGaAs permitti=13.85
material material=InGaAs AUGN=7e-29
material material=InGaAs AUGP=7e-29
material material=InGaAs MUP=450
material material=InGaAs alphaa=8000
material material=InGaAs copt=9.6e-11

Optical Properties of Materials

material material=InGaAs sopra=Ingaas.nk
material material=Inp sopra=Inp.nk

```
## Models #####
```

```
models fermi srh fldmob conmob optr print auger bgn
```

```
## Impact Ionization #####
```

```
impact selb
```

```
impact material=InP AN1=2.84e6
```

```
impact material=InP AP1=4.12e6
```

```
impact material=InP BN1=2.286e6
```

```
impact material=InP BP1=1.88e6
```

```
## Calculation Methods #####
```

```
method climit=1e-4
```

```
## Output Specification #####
```

```
output impac e.field jx.e jy.e jx.h jy.h opt.int con.band val.band
```

```
## Darck Current #####
```

```
solve init
```

```
log outf=APD822.log
```

```
log csvf=APD822.csv APPEND
```

```
solve vanode=-0.01
```

```
solve vanode=-0.1
```

```
solve vanode=-1 vstep=-0.1 vfinal=-80 name=anode
```

```
#comp=1e-5 cname=cathode
```

```
#solve vstep=-1 vfinal=-152 name=anode
```

```
save outf=APD822.str
```

```
#solve vstep=-1 vfinal=-160 name=anode
```

```
log off
```

```

#tonyplot APD822.str -set ElectricField.set

## Light Current #####

#beam num=1 wavelength=1.55 angle=90 x.ori=25 y.ori=-0.5

beam num=1 x.origin=25 y.origin=-0.1 angle=90.0 wavelength=1.55 rays=200 gaussian x.mean=-0.7
xsigma=5

solve init

solve b1=1e-04

solve b1=1e-03

solve b1=1e-02

solve b1=1e-01

solve b1=0.2

solve b1=0.3

solve b1=0.4

#solve init

#solve b1=1e-03

#solve b1=1e-02

#solve b1=1e-01

save outf=APD_P822.str

#tonyplot APD_P822.str -set PhotoGenerationRate.set

log outf=APD_P822.log

log csvf=APD_P822.csv APPEND

solve vanode=-0.01

solve vanode=-0.1

solve vanode=-1 vstep=-0.1 vfinal=-80 name=anode

#comp=1e-5 cname=cathode

#solve vstep=-1 vfinal=-160 name=anode

#log off

tonyplot APD822.log -overlay APD_P822.log -set apd_iv.set

quit

```